



1 **Regional and intercontinental pollution signatures on**
2 **modeled and measured PAN at northern mid-latitude**
3 **mountain sites**

4 Arlene M. Fiore^{1,2}, Emily V. Fischer³, Shubha Pandey Deolal⁴, Oliver Wild⁵, Dan
5 Jaffe^{6,7}, Johannes Staehelin⁴, Olivia E. Clifton^{1,2}, George P. Milly², Dan Bergmann⁸,
6 William Collins⁹, Frank Dentener¹⁰, Ruth M. Doherty¹¹, Bryan N. Duncan¹², Bernd
7 Fischer¹³, Stefan Gilge^{14,15}, Peter G. Hess¹⁶, Larry W. Horowitz¹⁷, Alexandru Lupu^{18,19},
8 Ian MacKenzie¹¹, Rokjin Park²⁰, Ludwig Ries²¹, Michael G. Sanderson²², Martin G.
9 Schultz²³, Drew T. Shindell²⁴, Martin Steinbacher²⁵, David S. Stevenson¹¹, Sophie
10 Szopa²⁶, Christoph Zellweger²⁵, Guang Zeng²⁷

11 ¹Department of Earth and Environmental Science, Columbia University, Palisades, NY, 10964, U.S.A.

12 ²Lamont-Doherty Earth Observatory of Columbia University, Palisades, NY, 10964, U.S.A.

13 ³Department of Atmospheric Science, Colorado State University, Fort Collins, CO, 80521, U.S.A.

14 ⁴Institute for Atmospheric and Climate Science, ETH Zürich, Switzerland

15 ⁵Lancaster Environment Centre, Lancaster University, Lancaster, LA1 4YQ, UK

16 ⁶School of STEM, University of Washington, Bothell, WA, 98011, U.S.A.

17 ⁷Department of Atmospheric Science, University of Washington, Seattle, WA, 98195, U.S.A.

18 ⁸Lawrence Livermore National Laboratory, Livermore, CA, 94550, U.S.A.

19 ⁹Department of Meteorology, University of Reading, Reading, RG6 6BB, UK

20 ¹⁰European Commission, Joint Research Centre, Ispra, I-21027, Italy

21 ¹¹School of GeoSciences, The University of Edinburgh, Edinburgh, EH9 3FF, UK

22 ¹²Atmospheric Chemistry and Dynamics Laboratory, NASA GSFC, Greenbelt, MD 20720, U.S.A

23 ¹³Federal Environment Agency (UBA), Schauinsland, 79254, Germany

24 ¹⁴Meteorological Observatory Hohenpeissenberg, German Meteorological Service (DWD),
25 Hohenpeissenberg, DE

26 ¹⁵now at DWD, Research Center Human Biometeorology, Freiburg, DE

27 ¹⁶Department of Biological and Environmental Engineering, Cornell University, Ithaca, NY, 14853, U.S.A.

28 ¹⁷Geophysical Fluid Dynamics Laboratory, National Oceanic and Atmospheric Administration, Princeton,
29 NJ, 08540, U.S.A.

30 ¹⁸Centre for Research in Earth and Space Science, York University, Toronto, M3J 1P3, Canada

31 ¹⁹now at Air Quality Research Division, Environment and Climate Change Canada, Toronto, M3H 5T4,
32 Canada

33 ²⁰School of Earth and Environmental Sciences, Seoul National University, Seoul, 08826, Republic of Korea

34 ²¹II4.5.7, German Environment Agency (UBA), Zugspitze, 82475, Germany

35 ²²Met Office, Exeter, EX1 3PB, UK.

36 ²³Jülich Supercomputing Centre, Forschungszentrum Jülich, 52425 Jülich, Germany

37 ²⁴Nicholas School of the Environment, Duke University, Durham, NC, 27708, U.S.A.

38 ²⁵Laboratory for Air Pollution / Environmental Technology, Empa – Swiss Federal Laboratories for
39 Materials Science and Technology, Dübendorf, CH-8600, Switzerland

40 ²⁶Laboratoire des Sciences du Climat et de l'Environnement, Institut Pierre Simon Laplace,
41 CEA/CNRS/UVSQ, Gif sur Yvette, France

42 ²⁷National Institute of Water and Atmospheric Research, Wellington, 6021, New Zealand

43
44 *Correspondence to:* Arlene M. Fiore (amfiore@ldeo.columbia.edu)
45

46 **Abstract.** Peroxy acetyl nitrate (PAN) is the most important reservoir species for nitrogen oxides (NO_x) in
47 the remote troposphere. Upon decomposition in remote regions, PAN promotes efficient ozone production.



48 We evaluate monthly mean PAN abundances from global chemical transport model simulations (HTAP1)
49 for 2001 with measurements from five northern mid-latitude mountain sites (four European and one North
50 American). The multi-model mean generally captures the observed monthly mean PAN but individual
51 models simulate a factor of ~4-8 range in monthly abundances. We quantify PAN source-receptor
52 relationships at the measurement sites with sensitivity simulations that decrease regional anthropogenic
53 emissions of PAN (and ozone) precursors by 20% from North America (NA), Europe (EU), and East Asia
54 (EA). The HTAP1 models attribute more of the observed PAN at Jungfraujoch (Switzerland) to emissions
55 in NA and EA, and less to EU, than a prior trajectory-based estimate. The trajectory-based and modeling
56 approaches agree that EU emissions play a role in the observed springtime PAN maximum at Jungfraujoch.
57 The signal from anthropogenic emissions on PAN is strongest at Jungfraujoch and Mount Bachelor
58 (Oregon, U.S.A.) during April. In this month, PAN source-receptor relationships correlate both with model
59 differences in regional anthropogenic volatile organic compound (AVOC) emissions and with ozone
60 source-receptor relationships. PAN observations at mountaintop sites can thus provide key information for
61 evaluating models, including links between PAN and ozone production and source-receptor relationships.
62 Establishing routine, long-term, mountaintop measurements is essential given the large observed
63 interannual variability in PAN.

64 **1 Introduction**

65 Ozone (O_3) distributions over northern mid-latitude regions reflect a combination of O_3 produced from
66 sources within a given region and O_3 transported from outside that region. Intercontinental influence on
67 surface O_3 levels occurs via at least two pathways: (1) O_3 can be produced within a polluted continental
68 boundary layer, ventilated to the free troposphere and efficiently transported to other continents; and (2) O_3
69 can also be produced in transit from the export and subsequent chemical evolution of precursors such as
70 peroxyacetyl nitrate (PAN) (Jaeglé et al., 2003; Kotchenruther et al., 2001a; Hudman et al., 2004). PAN
71 serves as a reservoir species for nitrogen oxides (NO_x), facilitating long-range transport of this chemical
72 family. To better understand differences in the quantification of O_3 transport, the Task Force on
73 Hemispheric Transport of Air Pollution (HTAP) organized a global model intercomparison exercise,
74 referred to here as HTAP1. A factor of two difference was identified in the HTAP1 model estimates of
75 surface O_3 response to changes in anthropogenic precursor emissions from continental-scale, northern mid-
76 latitude source regions (HTAP 2007; HTAP 2010). These precursor emissions include both NO_x and non-
77 methane volatile organic compounds (VOC) that produce PAN along with O_3 . Here, we take a first step
78 towards determining the extent to which source-receptor relationships for PAN and O_3 are related.
79 Specifically, we extend the prior HTAP1 analysis to evaluate lower tropospheric PAN distributions and to
80 quantify the impact of regional versus intercontinental anthropogenic emissions on PAN abundances.
81 Improved understanding of the processes controlling PAN abundances will help quantify the impact of
82 intercontinental transport on surface O_3 .

83



84 PAN is formed from the reversible reaction between acetyl peroxy radicals (CH_3COO_2) and nitrogen
85 dioxide (NO_2). Once formed, PAN can be lofted to the free troposphere, where it is more stable at colder
86 (lower) temperatures and can be efficiently transported throughout the hemisphere (Singh, 1987; Singh and
87 Hanst, 1981). The lifetime of PAN against thermal decomposition is about 1 hour at 20°C , and it
88 approximately doubles for every 4°C decrease in temperature. In the mid-troposphere during spring, when
89 intercontinental air mass flow is strongest, the lifetime of PAN is longer than a month. When PAN
90 decomposes in low- NO_x regions of the atmosphere, the NO_x released can produce O_3 up to eight times
91 more efficiently than in polluted (high- NO_x) regions (Liang et al., 1998; Liu et al., 1987). Several studies
92 emphasize the potential for PAN to increase the hemispheric NO_x burden and thus global O_3 abundances
93 (Moxim et al., 1996; Wang and Jacob, 1998), as O_3 formation is NO_x -limited in most of the free
94 troposphere (Chameides et al., 1992). Owing to the sensitivity of PAN thermal decomposition to
95 temperature, PAN also plays a role in altering the distribution of reactive nitrogen and hence O_3 under a
96 warming climate (e.g. Doherty et al., 2013). Efficient O_3 production in the lower troposphere following
97 subsidence of PAN-containing air masses has been observed during several aircraft field campaigns in the
98 Eastern Pacific and at mountain top sites in the Western U.S. and North Atlantic (Fischer et al., 2010;
99 Heald et al., 2003; Hudman et al., 2004; Kotchenruther et al., 2001a,b; Val Martin et al., 2008a; Zhang et
100 al., 2008).

101

102 The role of O_3 formation resulting from PAN chemistry by the two main pathways described above – via
103 PAN chemistry versus direct transport of O_3 formed in a remote boundary layer – in contributing to the
104 estimates of intercontinental source-receptor relationships for surface O_3 reported by HTAP (2010) is not
105 well quantified. Jaegle et al. (2003) provided a budget for the Pacific Northwest, suggesting that 28% of the
106 O_3 is associated with PAN-to- NO_x conversion in the Pacific free troposphere between 0-6 km. One regional
107 modeling study found that PAN export and its subsequent decomposition, followed by NO_x -induced O_3
108 formation, contributed 20% of the spatially averaged response of surface O_3 levels over East Asia to
109 European anthropogenic emission changes to (Lin et al., 2010). The same study found that this process may
110 contribute up to 50% of the O_3 response to European emission changes at mountain sites. A global
111 modeling study found that PAN produced from East Asian emissions and exported to the free troposphere
112 contributes 35% and 25% in spring and summer, respectively, to the free tropospheric O_3 abundance over
113 western North America (Jiang et al., 2016).

114

115 We hypothesize that PAN may serve as a sensitive diagnostic of model uncertainties in O_3 production
116 chemistry and transport (Emmerson and Evans, 2009; Kuhn et al., 1998), particularly given that model
117 errors in O_3 production may be buffered by compensating errors in O_3 losses. Prior analysis of
118 measurements and global model simulations suggests that PAN abundances at high altitude sites may be
119 more sensitive than O_3 itself to changes in precursor emissions (Fiore et al., 2011; Fischer et al., 2011; Jaffe
120 et al., 2007). We interpret this stronger sensitivity of PAN to changes in precursor emissions, as compared



121 to O₃, in terms of the relative independence of PAN loss pathways to changes in emissions. While PAN
122 production loosely mirrors much of the complex O₃ production chemistry, its dominant loss pathways are
123 much simpler than those for O₃. These PAN loss pathways are less likely to respond to changes in
124 emissions than those for O₃. PAN loss pathways include thermal decomposition (which dominates below
125 approximately 7 km); photolysis in the upper troposphere; and dry deposition within the boundary layer
126 (Kirchner et al., 1999; Roberts, 2007; Turnipseed et al., 2006). All of the HTAP1 models include PAN
127 formation, but the chemical mechanisms and kinetic rate coefficients differ, with likely implications for
128 long-range transport (Emmerson and Evans, 2009). More generally, PAN is a useful tracer of
129 photochemistry because of its low background and the absence of direct emissions.

130

131 For our analysis, we construct climatological monthly mean PAN abundances by compiling multi-year
132 PAN measurements at northern mid-latitude mountain sites and use them to evaluate monthly mean
133 abundances simulated with the models that participated in the HTAP1 project. We view this analysis as a
134 first step towards determining the extent to which model differences in PAN can provide insights into
135 model representation of processes that also influence intercontinental O₃ transport. While aircraft
136 observations have advanced the understanding of the chemistry and dynamics of individual plumes (e.g.,
137 Alvarado et al., 2010), their limited temporal coverage is not well suited for comparison with the HTAP1
138 monthly mean PAN mixing ratios. Similarly, the HTAP1 monthly mean mixing ratios are not well suited to
139 evaluation with tropospheric PAN column abundances retrieved from instruments aboard satellite platforms
140 (e.g., Payne et al., 2014) as these require application of retrieval-specific averaging kernels and a priori
141 profiles. These other observational platforms are likely to provide additional constraints on inter-model
142 discrepancies in coordinated multi-model efforts that archive three-dimensional fields at daily or higher
143 temporal frequency at the locations of aircraft flights and satellite overpasses.

144

145 We begin by describing the HTAP1 model simulations and mountaintop measurements (Section 2) before
146 quantifying the multi-model range of lower tropospheric PAN distributions, and evaluating this range with
147 available measurements at northern mid-latitude mountain sites (Section 3). We then focus on the
148 Jungfrauoch site in Europe to capitalize on a prior attribution of measured PAN mixing ratios to European,
149 North American, and East Asian emissions using trajectory-based methods (Pandey Deolal et al, 2013), and
150 compare these estimates with those derived from model sensitivity simulations (Section 4). We select one
151 European and one North American mountain site to probe relationships between simulated PAN and
152 regional emissions or transport in the individual models, with the goal of identifying some of the dominant
153 processes controlling hemispheric transport of PAN to these locations (Section 5) and examine the potential
154 relevance of conclusions regarding PAN origin to O₃ (Section 6). Finally, we summarize our conclusions
155 and offer a few recommendations for future work (Section 7).



156 2. Approach

157 In this section, we describe the HTAP1 model simulations (Section 2.1), the multi-year measurements of
158 PAN at five northern mid-latitude mountaintop sites, and our strategy to sample the models at these sites
159 (Section 2.2). We then describe the methodology used by Pandey Deolal et al. (2013) to derive trajectory-
160 based attributions of PAN measured at Jungfraujoch to East Asian, European, and North American source
161 regions, and discuss some limitations of this approach (Section 2.3). We use these trajectory-based source
162 attributions to evaluate the responses of PAN at Jungfraujoch to regional emission perturbations in the
163 HTAP1 model simulations.

164 2.1 HTAP1 model simulations

165 We use monthly mean PAN mixing ratios simulated by fourteen global chemistry transport models for the
166 2001 meteorological year (Table 1); the temporal resolution available for most three-dimensional chemical
167 fields in the HTAP1 model archive is limited to monthly. While simulations from Phase 2 of HTAP
168 (HTAP2) are available, they focus on meteorological years of 2008-2010. Given our interest in comparing
169 with the trajectory-based attribution of observations in 1997-1998 (Section 4) and the substantial changes
170 in NO_x emissions (a precursor to PAN) between the late 1990s and late 2010s (e.g., Hilboll et al., 2013), we
171 restrict our analysis to the HTAP1 year 2001 simulations.

172

173 We consider four HTAP1 Source-Receptor (SR) simulations (Table 2): a base case (denoted SR1, SR
174 simulation 1, for consistency with prior publications) and three perturbation simulations in which
175 anthropogenic O₃ precursor emissions (NO_x, VOC, carbon monoxide and aerosols) for the year 2001 are
176 reduced simultaneously by 20% within East Asia (SR6EA), Europe and northern Africa (SR6EU), and
177 North America (SR6NA). These three regions, depicted as white boxes in Figure 1, have been shown to
178 influence lower tropospheric O₃ (and PAN) at northern mid-latitudes more than the fourth HTAP1 region
179 (SR6SA; Jonson et al., 2010). We attribute PAN, sampled at mountaintop sites (see Section 2.2), separately
180 to emissions within these three source regions by differencing the perturbation and base simulations
181 (SR6XX-SR1, where XX refers to the region in which emissions of PAN precursors were decreased by
182 20%). We refer to this difference as the source-receptor relationship for PAN.

183

184 Of the models in Table 1, eleven used prescribed meteorological fields to drive tracer transport for the year
185 2001. Two models are chemistry-transport models coupled directly to a general circulation model forced by
186 observed sea surface temperatures (STOC-HadAM3 and STOCHEM) and one model incorporates
187 chemistry directly into a general circulation model (UM-CAM). We include results from these three models
188 here as their climatological nature matches that of our evaluation, which compiles PAN measurements
189 across several years. The individual model specifications and emissions are described in detail in Fiore et
190 al. (2009), with a summary of specifications and simulations relevant for our study provided in Tables 1



191 and 2. In HTAP Phase I, each model used its own emissions inventories (listed in Table A1 of Fiore et al.,
192 2009); Fiore et al. (2009) give emission totals within each HTAP Phase 1 source region for all (their Table
193 A2) and anthropogenic (their Table A3) emissions of NO_x, NMVOC, and CO. The relative inter-model
194 spread in regional anthropogenic emissions is smallest for NO_x emissions in EU and NA (<10%) and
195 largest for VOC from EU (58%) (Fiore et al. 2009). We conduct one additional simulation in the
196 MOZARTGFDL-v2 model, in which we increase North American isoprene emissions by 20% (ISOPNA;
197 described in Fiore et al., 2011), to demonstrate the sensitivity of PAN formation to isoprene emissions.

198

199 To separate the role of differences in model transport on simulated PAN from the combined impacts of
200 differences in model emissions and chemistry, we analyze an additional set of idealized tracer simulations
201 available from eleven models (see column COfromXX in Table 1, where XX is the source region). In these
202 simulations, a set of tagged carbon monoxide-like tracers are emitted, each from a single HTAP1 source
203 region with a 50-day lifetime, and with identical emissions across models. Biomass burning emissions for
204 the CO tracers are from GFED (van der Werf et al., 2006; 2010) and other emissions are from the RETRO
205 project (Schultz et al., 2007; 2008). We refer to these tracers as “COfromEA”, “COfromNA”, and
206 “COfromEU”, which denote the tracers emitted from EA, NA, EU, respectively (Table 2; see also Doherty
207 et al., 2013; Shindell et al., 2008).

208 **2.2 Multi-year PAN measurements at mountaintop sites and model sampling**

209 To evaluate the HTAP1 models, we compiled monthly climatologies of lower tropospheric PAN
210 measurements from northern mid-latitude mountain observatories (Table 3). Given the large interannual
211 variability in PAN abundances, we restricted our analysis to sites with at least two years of observations in
212 the same month, from which we estimate a monthly climatology for PAN to compare to the models. PAN
213 observations from Mount Bachelor (U.S.A.), Jungfrauoch (Switzerland), and Zugspitze
214 (Schneefernerhaus), Hohenpeissenberg, and Schauinsland (all in Germany) meet these criteria (Table 3).
215 Site locations are shown as white circles in Figure 1. Taken together, these mountaintop measurements
216 span 15 years, from 1995 to 2010, although only one site (Schauinsland) overlaps with the year 2001
217 chosen for the HTAP1 simulations.

218

219 PAN was measured at all five mountain sites using gas chromatography with electron capture detection
220 (ECD). A custom system using a Shimadzu Mini-2 ECD was employed at Mount Bachelor (Fischer et al.,
221 2010) and the commercially available Meteorologie Consult (GmbH) system was used at the European
222 sites (Zellweger et al., 2000). Calibrations were performed using a photochemical source where PAN is
223 generated from the photolysis of excess acetone and NO in air (Warneck and Zerbach, 1992; Volz-Thomas
224 et al., 2002). Reported detection limits are ~20 ppt for PAN measurements at Mount Bachelor, and ~50 ppt
225 for the European sites, with total uncertainties of <10% (Fischer et al., 2010; Zellweger et al., 2003).

226



227 We use monthly mean values at each of the measurement sites in order to match the temporal resolution of
228 PAN archived from the models. We include all available data at each site to calculate monthly means, and
229 do not filter the data for upslope winds or any other criteria. When measurements are below detection limit,
230 half the detection limit is used to calculate mean values. This assumption should not affect our conclusions
231 as PAN values below detection limit are generally observed in nocturnal boundary layers where PAN is
232 depleted by deposition whereas these high elevation sites generally sample free tropospheric air at night
233 (e.g., Weiss-Penzias et al., 2004). At Mount Bachelor, the cleanest of the 5 mountaintop sites used in
234 Figure 2, Fischer et al. (2010) have shown that the range of PAN measurements during springtime (our
235 focal season) is an order of magnitude larger than the amplitude of the diurnal cycle in PAN, suggesting
236 that PAN mixing ratios are not primarily controlled by diurnal wind patterns.

237

238 For comparison with the observations, we sample each model on its native grid (Table 1) at the horizontal
239 grid cell containing the latitude and longitude of each mountain site. Orography at these mountain sites is
240 poorly resolved at the relatively coarse HTAP1 model horizontal resolutions, and consequently the model
241 vertical grid differs from the real world. This mismatch requires us to apply some approximations for
242 sampling in the vertical. We convert the station altitude to an approximate pressure level by assuming a
243 mean tropospheric temperature of 260 K, which gives an atmospheric scale height of 7.6 km. We then
244 sample the models by linearly interpolating between the pressures of the two model grid cells that vertically
245 bound this pressure level, using the corresponding monthly pressure fields from each model. While
246 different sampling strategies may alter the exact value of simulated PAN and its comparison to
247 observations, our primary interest is in the inter-model differences. Although the Zugspitze and
248 Hohenpeissenberg sites fall within the same horizontal grid cell due to the coarse horizontal resolution of
249 the HTAP1 models, the station altitudes differ, so we consider the two sites separately.

250 **2.3 Trajectory-based attribution of PAN measurements at Jungfraujoch to emission region**

251 Trajectories were calculated from 6 hourly wind fields from ECMWF (European Centre for Medium-Range
252 Weather Forecasts) ERA Interim reanalysis data. The trajectory-based source attribution to a given region
253 is determined by averaging PAN mixing ratios every six hours on days when 20-day back-trajectories can
254 be unambiguously assigned to the continental source region based on recent boundary layer contact. The
255 values for PAN attributed to a given source region represent the mean mixing ratios on days with
256 trajectories attributed to the boundary layer over that source region, weighted by the frequency of
257 trajectories originating in that source region as described by Pandey Deolal et al. (2013). The observed
258 fractional attribution is estimated as the frequency-weighted values divided by the observed monthly
259 means.

260

261 A limitation of this trajectory-based source attribution is that the lifetime of PAN often exceeds the time
262 scale over which the back trajectories can be used to trace PAN observed at Jungfraujoch back to its



263 original continental boundary layer source. Pandey Deolal et al. (2013; see their Figure 1) label these cases
264 as “free troposphere” and find that 13-32% (range depends on season and year) of all trajectories fall in this
265 category. Uncertainties in trajectory calculations normal to the direction of flow are typically about 20% of
266 the horizontal distance traveled and thus increase with time (Pandey Deolal 2013; Stohl, 1998). As
267 trajectory uncertainties vary from case to case, an ensemble of backward trajectories is calculated at
268 Jungfraujoch to reduce error. Given the dependence of uncertainty on trajectory length, constraints from the
269 trajectory-based approach are likely to be stronger for the regional European emission influence than for
270 the more distant source regions of North America and East Asia.

271

272 The trajectory-based approach assumes that all PAN in an air mass that originates over a continent is
273 produced from PAN precursor emissions (NO_x and VOC) over that continent and may thus overestimate the
274 influence from that particular source region if there are non-trivial enhancements to PAN in the air mass
275 produced by emissions in other regions. On the other hand, the “free troposphere” air masses must contain
276 some influence from global PAN precursor emissions, which would tend to cause the trajectory-based
277 approach to underestimate the influence from any source region. In contrast, the HTAP1 model
278 perturbation simulations directly diagnose the impact of precursor emissions within a given source region
279 to the PAN simulated at the Jungfraujoch site. We interpret the trajectory-based attributions as likely
280 offering a lower limit for the intercontinental influence from NA and EA at Jungfraujoch and an upper limit
281 for PAN originating from the EU source region. Despite the limitations outlined here, this trajectory-based
282 approach offers one of the only available independent methods for evaluating source-receptor relationships
283 diagnosed with the global HTAP1 models. Evaluating emission-response relationships is critical to build
284 confidence in using these models to project responses to future emission changes.

285 **3. Modeled and measured lower tropospheric PAN at northern mid-latitudes**

286 At northern mid-latitudes, intercontinental pollutant transport maximizes in spring (e.g., HTAP 2010).
287 Earlier work attributed the observed springtime maximum in tropospheric PAN to the build-up of longer-
288 lived precursors during the northern hemisphere winter and subsequent PAN production during spring as
289 photochemical activity rises; at the same time, colder temperatures during spring slow the PAN
290 decomposition rate relative to the warmer summer months (Bottenheim et al., 1994; Penkett and Brice,
291 1986; Schmitt and Volz-Thomas, 2004). At Jungfraujoch, the highest springtime PAN levels have been
292 shown to occur in air masses originating in the European planetary boundary layer (Pandey Deolal et al.,
293 2013, 2014). This maximum in EU influence reflects strong photochemical activity in spring, enhanced
294 thermally induced vertical transport from the European boundary layer, and a longer PAN lifetime against
295 thermal decomposition relative to the warmer summer season. Smaller springtime maxima occur in free
296 tropospheric air masses, implying a larger role for regional pollution in contributing to the observed
297 springtime maximum in PAN than previously recognized (Pandey Deolal et al., 2013, 2014).

298



299 We examine simulated PAN distributions during April and July in the northern hemisphere to illustrate
300 characteristic differences in the spring versus summer distributions as represented by the model ensemble
301 mean PAN mixing ratios at 650 hPa (~3 km), the level sampled by the three highest altitude sites in Table
302 2. Higher mixing ratios and a stronger latitudinal gradient are evident in April as compared to July (Figure
303 1 left column). Compared to April, the lower PAN mixing ratios downwind of source regions in July reflect
304 the shorter lifetime of PAN at warmer temperatures. In both seasons, enhancements occur over the major
305 source regions of the eastern United States and Mexico, Europe, and Asia. The southward extension of
306 higher PAN mixing ratios over North America in July as compared to April reflects (1) the impact of
307 biogenic PAN precursors, such as emission of isoprene and its subsequent oxidation to products including
308 methyl glyoxal and acetaldehyde (Fischer et al., 2014; Roberts et al., 2006; Wolfe et al., 2009), and (2)
309 active convection and the associated lightning NO_x in the warmer summer months.

310

311 The multi-model relative standard deviations (the coefficient of variation: the standard deviation over the
312 14 models divided by the model ensemble mean) are also shown in Figure 1 (right column; note we set a
313 100 ppt PAN threshold level to emphasize variability across the models in locations with higher PAN
314 mixing ratios). The multi-model spread in lower tropospheric PAN (at 650 hPa) in April mainly follows a
315 latitudinal gradient, with less inter-model deviation at high-latitudes where PAN is most abundant and more
316 inter-model deviation at lower latitudes where PAN mixing ratios are lower. The higher inter-model spread
317 in remote regions reflects not only differences in model representations of PAN formation, but also
318 differences in transport and subsequent thermal decomposition. In April, the inter-model relative standard
319 deviations over Europe exceed 50%, suggesting that the European mountain sites may be particularly
320 useful to test the models. In summer, variability across the models is largest in the North Pacific off the
321 Alaskan Aleutian islands, off the west coast of Mexico, and over the Atlantic centered at about 30°W and
322 30°N, near the Pico Mountain, Azores site (e.g., Honrath et al., 2004; Val Martin et al., 2008ab). Future
323 measurements in regions where model variability is large would provide constraints on PAN distributions
324 in the models, and on the relative influence from different source regions on PAN, as discussed below.

325

326 Observed PAN mixing ratios at the northern mid-latitude mountain sites tend to be highest in spring
327 (Figure 2), consistent with remote measurements at lower elevations in the northern hemisphere
328 (Bottenheim et al., 1994; Penkett and Brice, 1986; Singh and Salas, 1989). Substantial year-to-year
329 variability (black vertical bars in Figure 2) is evident from the measurements (Zellweger et al., 2003;
330 Fischer et al., 2011; Pandey Deolal et al. 2013, 2014). Capturing this interannual variability would be a
331 useful test for future multi-year modeling efforts. On average, the measurements at all sites (black circles)
332 indicate that the spring peak occurs in April. An exception occurs at Schauinsland in 2001 (blue triangles),
333 when the peak is delayed until May, and a secondary peak occurs in August. Consistent with the
334 measurements, the 2001 multi-model mean is highest in April at Mount Bachelor and Zugspitze, but occurs
335 in May at Schauinsland, although in early spring the multi-model mean abundance falls closer to the multi-



336 year average of the measurements than the low values measured in 2001. Jungfraujoch lacks measurements
337 in 2001 but the measured inter-annual variability is largest in May. The large observed variability at
338 Jungfraujoch indicates that there are individual years where PAN at Jungfraujoch peaks in May. The
339 models suggest that a May peak occurred during 2001 at Jungfraujoch, similar to the observations and
340 multi-model mean at Schauinsland. At Hohenpeissenberg, the measurements peak in April, but the models
341 indicate a broad spring-summer maximum with higher PAN abundances than measured as well as a
342 September peak. This low elevation site may be more susceptible to the influence of boundary layer PAN
343 formation from European emissions (e.g., Gilge et al., 2010; Kaiser et al., 2007; Naja et al., 2003; Pätz
344 et al., 2000), and we interpret the model overestimate at Hohenpeissenberg as evidence that the models cannot
345 properly resolve the vertical gradients in PAN. This shortcoming could in part reflect inadequate dry
346 deposition (e.g., Turnipseed et al., 2006), and thus an overestimate of European boundary layer influence
347 on the magnitude and seasonality of PAN abundances.

348

349 Individual model simulations indicate a wide spread across the models (gray shading in Figure 2).
350 Systematic biases versus the observations are evident in some models. For example, the CAM-Chem model
351 simulates PAN abundances that are usually higher than observed mixing ratios (brown line in Figure 2),
352 and than most of the other models, whereas PAN abundances simulated by GISS-modelE are always low
353 during summer (green line in Figure 2). Monthly mean PAN abundances in the GMI-v0f (cyan) and
354 MOZART2-GFDL (red) models, however, do not consistently follow the same ranking from site to site.
355 Overall, the multi-model mean (dashed line) generally falls close to the monthly mean observed mixing
356 ratios with a tendency towards a positive bias at Mount Bachelor in all seasons (within ~50 ppt) and at
357 Hohenpeissenberg in the warm season.

358 **4. Evaluation of regional and intercontinental influences on PAN at Jungfraujoch**

359 We apply the trajectory-based estimates of the contributions from emissions within EU, NA, and EA to
360 PAN measured at Jungfraujoch (Pandey Deolal et al., 2013; described in Section 2.3) to evaluate the PAN
361 source-receptor relationships simulated by the HTAP1 models. For this comparison, we multiply the PAN
362 source-receptor relationships (SR1-SR6XX; Section 2.1 and Table 2) by a factor of 5 to scale from the 20%
363 emission perturbations to 100%. Our linear scaling of the PAN response from 20% to 100% emission
364 perturbations may incur errors due to non-linear chemistry. To assess the magnitude of this error, we
365 analyze an additional simulation with the FRSGUCI model that sets European anthropogenic emissions of
366 NO_x, CO and VOC to zero (a 100% perturbation). We find that assuming linearity in the PAN response to
367 European emission changes (20%*5 vs. 100%) incurs an error of ~10% over the EU emission region and
368 <3% over other regions. Earlier work assessing linearity in O₃ responses also indicates stronger non-
369 linearity to regional versus intercontinental sources (Fiore et al., 2009; Wu et al., 2009; Wild et al., 2012).
370 Although PAN and O₃ share the same precursor emissions, O₃ responds more strongly to changes in NO_x
371 emissions outside of high-NO_x regions, whereas PAN is sensitive to changes in both NO_x and VOC



372 emissions, and in many regions PAN responds more strongly to changes in VOC emissions (Fischer et al.,
373 2014; see their Figure 4). The sensitivity of PAN to changes in VOC emissions can be amplified by a
374 chemical feedback in remote regions where PAN is the main NO_x source: in these regions, if PAN
375 decreases then O₃ decreases, which lowers the [NO₂]/[NO] ratio that controls PAN formation, thereby
376 reducing the effective PAN lifetime (Fischer et al., 2014).

377

378 Figure 3 shows the observation-derived source attributions with those estimated by the model ensemble, for
379 both absolute (left column) and relative (right column) influences of precursor emissions from EU, NA, and
380 EA on PAN. The relative (fractional) contributions are obtained by dividing the absolute source-receptor
381 relationships by the total PAN mixing ratio in the SR1 simulation. Data in months with multiple years of
382 observations (April and May) show that the trajectory-based estimates for a given emission region can vary
383 from year to year by up to a factor of two for the PAN abundance attributed to that region, and by over 20%
384 for the relative attribution. The HTAP1 model estimates span an even larger range than the trajectory-based
385 estimates from two different years.

386

387 Of all the back-trajectories from Jungfraujoch, up to 40% originated in EU, 10-20% originated in North
388 America and fewer than 4% originated in EA (Pandey Deolal et al., 2013), consistent with the relative
389 ranking of multi-model mean source-receptor relationships for PAN from these two regions in Figure 3.
390 The multi-model mean is generally lower than the trajectory-based attribution to EU in late spring and
391 summer, possibly resulting from an inadequate model representation of local valley-mountain (upslope)
392 flows, which typically peak during these seasons (Pandey Deolal et al., 2013). For the intercontinental
393 source regions, all of the models exceed the estimates from the trajectory-based approach outside of the
394 warm season, with the exception of PAN from EA during October. Overall, the absolute trajectory-based
395 attributions of PAN at Jungfraujoch to intercontinental emissions fall close to the multi-model mean
396 estimate for the NA region from May through September and for the EA region in October (Figure 3).
397 Simulated fractional contributions of PAN produced from NA anthropogenic emissions are higher than the
398 trajectory-based estimates (with the exception of September) as expected given the inability of the
399 trajectory-based approach to attribute all measurements to a source region. Nevertheless, if the trajectory-
400 based attribution in Figure 3 provides a lower limit for the EA and NA source regions and an upper limit
401 for the EU source region (Section 2.3), then these two approaches (trajectory-based versus perturbation
402 simulations in the HTAP1 models) to determining the influences of regional versus intercontinental sources
403 on PAN measured at Jungfraujoch are consistent.

404

405 The higher PAN abundances in the HTAP1 models during the cold season reflect the long lifetime of PAN
406 at cold temperatures, which far exceeds the 20-day trajectory time scale. When the PAN lifetime exceeds
407 20 days, the trajectory-based approach cannot link the PAN measured at Jungfraujoch to a specific
408 continental boundary layer. We attribute the apparent mismatch in the seasonal cycle in the NA influence



409 on PAN at Jungfraujoch (Figure 3) to this shortcoming of the trajectory-based approach. Given the
410 substantial year-to-year variability in the monthly mean measurements, stronger constraints could be placed
411 on inter-model discrepancies if the model and trajectory-based attribution approaches used the same
412 meteorological year.

413

414 The absolute range of the PAN source-receptor relationships in the HTAP1 models is wide for all three
415 source regions (Figure 3, left). The inter-model spread in the fractional attribution is smaller for NA than
416 for the nearby EU region (Figure 3, right). The models rank differently in their estimates for absolute
417 versus relative attribution of PAN to anthropogenic emissions from the three regions. For example, the
418 typically high (brown curves in Figure 3) and lower (green curves in Figure 3) models agree more closely
419 on the relative attribution despite the large discrepancies in their simulated total PAN abundances (Figure
420 2) and in the absolute amount of PAN attributed to EU and NA sources. We conclude that constraints on
421 both absolute and relative ranges of source-receptor relationships are useful as some of the inter-model
422 range in PAN source-receptor relationships reflects differences in the mean state simulations that cancel out
423 in the fractional estimates.

424

425 In the future, as climate warms and anthropogenic emission controls continue to be phased in, we expect an
426 increasing role for temperature-sensitive PAN precursors such as biogenic VOC (BVOC). As an example,
427 we quantify the relative role of BVOC versus AVOC in contributing to intercontinental PAN source-
428 receptor relationships at Jungfraujoch in 2001. Specifically, we use an additional perturbation simulation
429 from a single HTAP1 model (MOZART2-GFDL; shown in red in Figures 2 and 3) in which isoprene
430 emissions were increased by 20% over NA, as might occur as climate warms, and compare the influence of
431 BVOC on PAN with the influences determined from the 20% decreases to anthropogenic emissions from
432 the three mid-latitude HTAP1 source regions (i.e., ISOPNA-SR1 for comparison with the magnitude of
433 SR1-SR6XX; we multiply these differences by a factor of 5 to estimate a 100% contribution in Figure 4).
434 In this model, a 20% increase in NA isoprene emissions exerts an influence on PAN at Jungfraujoch
435 roughly equivalent to a 20% reduction to NA anthropogenic NO_x, CO and VOC emissions from June-
436 November, or to a 20% decrease in EU anthropogenic emissions in June and August (Figure 4). The
437 intercontinental isoprene influence exceeds that from EA anthropogenic emissions throughout the warm
438 season. Fischer et al. (2014) find that contributions to PAN over Europe from BVOC emissions and from
439 lightning NO_x both peak in summer in the GEOS-Chem model (see their Figure 7). Other studies have also
440 noted strong impacts on PAN from lightning and biomass burning emissions (e.g., Fadnavis et al., 2014;
441 Fischer et al., 2011; Real et al., 2010; Zhu et al., 2015). We conclude that interpretation of both
442 summertime measurements and differences across models requires consideration of PAN precursors from
443 biogenic, lightning, and biomass burning sources. Springtime measurements of PAN, however, should
444 reflect more directly the influence of anthropogenic emissions.



445 **5. Factors contributing to the inter-model range in PAN source-receptor relationships**

446 In this section, we aim to advance our understanding of the factors contributing to model differences in the
447 PAN response to continental-scale emission changes. Our approach is to (1) examine the spread in source-
448 receptor relationships for PAN at Mount Bachelor in North America and Jungfraujoch in Europe, and (2)
449 link these to model differences in emissions or transport. We first identify months where the anthropogenic
450 emission influence on PAN is strongest. The HTAP1 multi-model ensemble mean values indicate that 80-
451 86% of the total multi-model mean PAN abundances at the two sites in January through April are produced
452 from anthropogenic emissions (NO_x , VOC, and CO) within the three northern mid-latitude source regions
453 (Figure 5). During boreal summer, this contribution drops to only 40-60% (Figure 5) due to the additional
454 influences from lightning NO_x , biogenic, and biomass burning emissions of PAN precursors (e.g., see NA
455 isoprene source in Figure 4). These warm season sources complicate our efforts to disentangle the role of
456 inter-model differences in anthropogenic emissions versus transport on simulated PAN source-receptor
457 relationships. In April, however, intercontinental pollution influence is highest in the multi-model ensemble
458 (the minimum in the difference between the dashed and solid black lines in Figure 5). The inter-model
459 differences in PAN abundances thus contain the strongest signals tied to inter-model variations in
460 anthropogenic precursor emissions in April. We focus our remaining analysis on April to probe more
461 deeply the inter-model differences in PAN responses at the two mountaintop sites to changes in
462 anthropogenic emissions.

463

464 We assess the importance of model differences in regional anthropogenic NO_x and NMVOC inventories
465 and transport in contributing to the spread across the simulated source-receptor relationships (gray shading
466 in Figure 3 at Jungfraujoch). At each site, we examine the correlation between simulated PAN attributed by
467 each model to anthropogenic emissions of VOC (AVOC; Figure 6) or NO_x . We find that the inter-model
468 range in a given regional AVOC emissions explains as much as 64% of the variation in PAN attributed to
469 EU emissions, and about 25% of the variance in PAN attributed to the NA region (Figure 6). The
470 relationships for the EA source-receptor relationships are not significant. In contrast to AVOC, we find
471 little relationship between the range in simulated PAN source-receptor relationships at the mountain sites
472 and the model spread in regional ANO_x emissions. Differences in model transport (e.g., Arnold et al., 2017;
473 Orbe et al., 2017) may also contribute to the inter-model differences in PAN source-receptor relationships.
474 Our analysis of the HTAP1 idealized CO tracers (Section 2.3) reveals little correlation between inter-model
475 differences in these idealized tracers and in PAN source-receptor relationships sampled at Mount Bachelor
476 and Jungfraujoch. Fischer et al. (2014) have previously shown that PAN abundances respond more strongly
477 to changes in emissions of VOC than of NO_x . Our analysis supports that earlier finding and highlights a key
478 role for model differences in regional AVOC emissions in contributing to the inter-model range in PAN
479 source-receptor relationships.

480



481 To investigate further these inter-model differences in PAN source-receptor relationships, we consider next
482 the importance that one model ascribes to a given source region relative to another source region. We first
483 examine the relative importance of emissions within the source region where the measurement site is
484 located versus the upwind intercontinental source region on PAN, by comparing NA:EA at Mount Bachelor
485 and EU:NA at Jungfraujoch. At Mount Bachelor, the HTAP1 multi-model mean source-receptor
486 relationships from NA, EA, and EU, are roughly equal in April (Figure 5). The differences across the
487 HTAP models in the relative importance of the NA:EA source regions on PAN (which range from about
488 0.5 to 2.5) correlate roughly equally with the ratio of the NA:EA transport tracers and with the ratio of the
489 NA:EA AVOC emissions (Spearman rank correlation coefficient (r) = 0.6 for both cases; Figure 7 left
490 column). We find no relationship with the ratio of the NA:EA ANO_x emissions. At Jungfraujoch, the
491 HTAP1 multi-model mean attributes much of the PAN to emissions from the EU and NA source regions
492 during April (Figure 5). The ratio of PAN attributed to EU versus NA at Jungfraujoch, however, varies
493 from approximately 0.5 to 2 across the individual HTAP1 models (Figure 7; right column). In contrast to
494 our findings at Mount Bachelor, this ratio at Jungfraujoch depends most strongly on the ratio of ANO_x
495 emissions in the EU to NA regions (r = 0.6), and more weakly on the ratio of EU:NA AVOC emissions (r =
496 0.5). The correlation is even weaker between the ratio of PAN source-receptor relationships for these two
497 regions with inter-model differences in transport as diagnosed with the CO tracers from EU versus NA (r =
498 0.4).

499

500 We next examine links between inter-model differences in ratios of ANO_x emissions, AVOC emissions, or
501 the transport tracers, with the ratio of PAN source-receptor relationships from two intercontinental regions.
502 At Mount Bachelor, the EU and EA source regions contribute similar amounts to multi-model mean PAN
503 during April (Figure 5). Across the individual models, however, the ratio of the EU to EA source region on
504 PAN at Mount Bachelor varies from less than half to a factor of two (Figure 8, left column). We find that
505 the ratio of PAN attributed to the EU versus EA source regions at Mount Bachelor correlates strongly
506 across the models with the ratio of the anthropogenic volatile organic compound (AVOC) emissions in the
507 respective source regions (r = 0.8; Figure 8). In contrast, the ratio of EU:EA anthropogenic emission
508 influence on PAN at Mount Bachelor shows little correlation with the respective regional NO_x emissions
509 used in the models, or with the differences in the simulated transport tracers (r = 0.3 for both cases; Figure
510 8). As at Mount Bachelor, the model spread in the contribution to total simulated PAN from the EA versus
511 NA source regions at Jungfraujoch depends most on the regional AVOC ratios (r = 0.8; Figure 8 right
512 column), with little correlation with inter-model differences in NA:EA ANO_x emissions. Some correlation
513 appears to exist between the NA:EA source-receptor relationships for PAN and the NA:EA transport
514 tracers (r = 0.6; Figure 8), although this weakens (to r = 0.5) if we exclude the left-most outlier. Finally, the
515 individual symbols in Figures 7 and 8 depict the meteorological fields used in each model; there is no
516 obvious relationship between PAN source-receptor relationships and the choice of meteorological fields, as
517 expected from our analysis of the idealized CO tracers.



518

519 For source-receptor pairs with significant relationships in Figures 6-8, the inter-model differences generally
520 correlate most strongly with differences in model AVOC emission inventories. What we attribute here to
521 AVOC emissions actually represents the combination of those emissions plus the subsequent chemistry that
522 those emissions undergo prior to producing PAN. Even if models use the same AVOC emissions,
523 differences in chemical mechanisms are likely to contribute to inter-model differences in PAN (Emmerson
524 and Evans, 2009). The AVOC emissions implemented in the HTAP1 models range by a factor of 5 for NA
525 and EA, and nearly a factor of 10 for EU. Our results indicate that constraints on the amount of VOC
526 emitted, and the PAN produced during oxidation of these VOCs, would narrow the range across model
527 estimates for PAN source-receptor relationships during April. Fischer et al. (2014) also emphasize the
528 sensitivity of global PAN budgets to AVOC emission inventories, which do not frequently receive much
529 attention in terms of model evaluation. Independent methods to derive source-receptor relationships from
530 observations, such as the trajectory-based approach in Section 4 are also needed to evaluate model
531 responses to emission changes, as opposed to abundance-based evaluations. Finally, while model
532 differences in transport may not contribute most to the multi-model spread in the monthly mean source-
533 receptor relationships examined here, we expect that transport would play a role in inter-model differences
534 in resolving individual trans-oceanic transport events.

535 **6. Links between PAN and O₃ source-receptor relationships**

536 We address here the extent to which observational constraints on PAN source-receptor relationships might
537 also serve to narrow the range of uncertainty in the inter-model spread in intercontinental source-receptor
538 relationships for O₃ (e.g., Fiore et al., 2009). We expect some commonality between the sensitivity of PAN
539 and O₃ to changes in precursor emissions because (1) both species are produced from chemical reactions
540 involving NO_x and VOC, and (2) PAN serves as a NO_x reservoir, which upon decomposition releases NO_x
541 that can then produce O₃ far downwind of the region where the PAN (and O₃) precursors were originally
542 emitted.

543

544 Earlier work found that inter-model differences in intercontinental influences on continental-scale surface
545 O₃ in the HTAP1 models correlate with the wide range of AVOC emissions used in the models, particularly
546 over the EU (Fiore et al., 2009). Our analysis in Section 5 also showed a dependence of inter-model
547 variations in the amount of PAN produced by (and transported from) a region on the magnitude of the
548 regional AVOC emissions. When we repeat the analysis in Figure 6 but for O₃, considering the influence
549 of the three source regions on two mountain sites (six total source-receptor pairs), we find little relationship
550 between the spread in the simulated O₃ source-receptor relationships and in the magnitude of the AVOC
551 emissions from the source region. Similar to our findings for PAN, the O₃ source-receptor relationships
552 show little correlation with the model range in regional ANO_x emissions. Model differences in transport, as
553 diagnosed with the regional idealized CO tracers, are generally not correlated with the inter-model spread



554 in PAN or O₃ source-receptor relationships. The correlation with these tracers, although weak, is higher for
555 O₃ than for PAN for all source-receptor pairs. A stronger correlation with the CO tracers does occur for the
556 influence of EU emissions on O₃ at Jungfraujoch. Overall, this analysis supports our hypothesis that PAN is
557 more sensitive to changes in emissions (and subsequent chemistry), particularly for VOC precursors, than
558 O₃.

559

560 We now assess more directly the extent to which the inter-model range in source region influence on
561 mountaintop PAN levels (Figure 3) is relevant for interpreting O₃ source-receptor relationships in the
562 HTAP1 models. We maintain our focus on April, when the signal from anthropogenic precursor emissions
563 on PAN is at its seasonal peak according to the models. Figure 9 illustrates our correlation analysis of PAN
564 and O₃ source-receptor relationships at Jungfraujoch and Mount Bachelor across the 12 models (SR1-
565 SR6XX where XX = EA, EU, or NA). Relationships vary across the individual source-receptor pairs, with
566 the inter-model variability in PAN explaining 16-60% of the inter-model differences in O₃ at the mountain
567 sites. The strongest relationships occur for the influence of regional sources on these mountain sites: NA at
568 Mount Bachelor and EU at Jungfraujoch. Intercontinental source-receptor pairs for O₃ and PAN at Mount
569 Bachelor are also significant to within 90%, with variability in the PAN attributed to intercontinental
570 source regions explaining 25-35% of the variability in the corresponding O₃ source-receptor relationship.

571

572 The correlations between PAN and O₃ source-receptor relationships could reflect a role for PAN transport
573 in contributing to O₃ production over the receptor region, or may instead reflect co-production of PAN and
574 O₃ from oxidation of regional precursor emissions followed by transport in the same air mass. In the latter
575 case, PAN is serving as a proxy for O₃ transport whereas in the former case, PAN is serving as the actual
576 pathway by which O₃ is transported. We do not have model diagnostics that allow us to distinguish
577 between these two roles for PAN. The correlations between PAN and O₃ source-receptor relationships,
578 however, suggest that long-term PAN measurements contain signals relevant for constraining the relative
579 importance of regional vs. intercontinental emissions on both PAN and O₃.

580 7. Conclusions and recommendations

581 We investigated monthly mean PAN mixing ratios from a suite of multi-model sensitivity simulations
582 coordinated by the Task Force on Hemispheric Transport of Air Pollution (HTAP, 2007; 2010; Table 1) in
583 conjunction with mountaintop measurements (Table 3) to quantify the influence of regional versus
584 intercontinental anthropogenic emissions on PAN at these sites. PAN transport and subsequent
585 decomposition leads to O₃ production, one pathway for intercontinental O₃ transport. Correlations between
586 inter-model differences in PAN and O₃ responses to perturbations in regional anthropogenic emissions
587 (e.g., EU at Jungfraujoch and NA at Mount Bachelor; Figure 9) imply that constraints on PAN should
588 reduce uncertainty in estimates of O₃ source-receptor relationships. As the O₃ response to climate warming



589 is partially dependent on thermally-sensitive PAN (e.g., Doherty et al., 2013), better constraints on PAN are
590 also needed to increase our confidence in the projected responses of O₃ to climate change.

591

592 The wide range in PAN levels, and its source-receptor relationships, across the HTAP1 models indicates a
593 need to improve our understanding of the chemical and physical mechanisms underlying PAN distributions
594 and seasonal cycles in the troposphere. Uncertainties in emissions as well as yields of PAN from VOCs,
595 both natural and anthropogenic, hinder a full understanding of PAN in the troposphere (Figure 6; see also
596 Fischer et al., 2014). Regional AVOC emissions usually differ more than NO_x emissions (e.g., Figures 7
597 and 8), and have fewer observational constraints (e.g., NO₂ columns are routinely retrieved from space).
598 The range in model representations of VOC chemistry also contributes to inter-model differences in PAN
599 (e.g., Emmerson and Evans, 2009).

600

601 To further our understanding of PAN in the troposphere, we recommend rigorous process-oriented
602 evaluation of models, both event-based (e.g., Fischer et al., 2010; Alvarado et al., 2010) and long-term
603 statistical evaluations of PAN and its relationships with other species. Ongoing multi-model projects,
604 including HTAP Phase 2 (HTAP2), the Chemistry-Climate Model Initiative (CCMI), and the upcoming
605 AerChemMIP simulations, may prove useful for some of this analysis. Accurate diagnosis of the impact of
606 differences in NO_x and VOC emissions on PAN and O₃ source-receptor relationships, however, hinges on
607 the availability of dedicated source attribution diagnostics or emission perturbation simulations, and would
608 also benefit from the availability of chemical budget diagnostics.

609

610 Multi-year PAN records at existing measurement sites would provide much needed constraints on PAN
611 production and export from the three major anthropogenic source regions at northern mid-latitudes (East
612 Asia, Europe, and North America). We identified only five multi-year datasets at mountain sites, four of
613 which are located near each other in Europe, and only one of which continues at present (Schauinsland). In
614 addition to the sites in Table 3 where PAN has been measured for at least two years, we suggest that PAN
615 measurements at other existing sites are needed to better constrain export from the North American and
616 Asian continents and subsequent trans-oceanic transport. The Tropospheric Ozone Assessment Report
617 (TOAR) database (Schultz et al., 2017) contains O₃ measurements from more than 60 stations at altitudes
618 above 2500 m, a useful starting point for identifying sites where observational constraints would best
619 discriminate across models (e.g., where the models vary most in Figure 1). Adding PAN to the suite of
620 species measured routinely aboard commercial aircraft (Ekstein et al., 2017; Petzold et al., 2015) would
621 also enable knowledge of PAN distributions across much of the northern mid-latitude free troposphere.
622 Although in their infancy, new satellite products for PAN offer much potential for documenting PAN
623 distributions, particularly in the upper troposphere, as well as temporal variability and trends across the
624 globe (e.g., Fadnavis et al., 2014; Jiang et al., 2016; Payne et al., 2014; 2017; Zhu et al., 2015; 2017).
625 Sampling models in a fully consistent manner with satellite-derived tropospheric PAN columns, along



626 aircraft flight tracks, or at long-term monitoring sites requires archiving model fields at high temporal
627 frequency at the measurement locations.

628

629 The substantial inter-model differences in PAN abundances and their attribution to regional anthropogenic
630 emissions identified here highlight the potential for observations of PAN to provide much-needed
631 constraints on model estimates of intercontinental transport. Seasonal and inter-annual variability in the
632 signal strength from anthropogenic (largest in spring at northern mid-latitudes) versus other sources
633 suggests process-level information for testing models can be obtained from careful interpretation of
634 seasonal cycles. Changes in meteorology and biomass burning (Fischer et al., 2011; Zhu et al., 2015) such
635 as those driven by ENSO (Koumoutsaris et al., 2008), as well as biogenic and lightning sources (Payne et
636 al., 2017), will also cause PAN to vary from one year to another and are expected to change as climate
637 warms. Springtime PAN measurements are most likely to resolve model discrepancies in anthropogenic
638 emission influences on PAN, whereas summertime measurements are strongly influenced by biogenic,
639 lightning, and biomass burning influences. We conclude that long-term observations of PAN in the free
640 troposphere during spring, although currently limited, could be a keystone measurement for improving
641 model simulations of intercontinental pollutant transport.

642 **Acknowledgments**

643 We thank Mathew Evans (York University, UK) and Terry Keating (U.S. EPA) for useful discussions.
644 AMF acknowledges NASA MAP (NNX14AM38G). DSS acknowledges NERC (grants NE/K001329/1 and
645 NE/N003411/1) and the ARCHER UK National Supercomputing Service (<http://www.archer.ac.uk>). Data
646 for the Mt. Bachelor Observatory are archived and available at the University of Washington data archive:
647 <https://digital.lib.washington.edu/researchworks/browse?type=subject&value=Mt.+Bachelor+Observatory>.
648 The PAN data for the European Mountain sites is archived by the World Data Centre for Greenhouse Gases
649 (<http://ds.data.jma.go.jp/gmd/wdcgg/>). Upon publication, all model fields and data used to generate the
650 figures will be placed in the CSU digital repository that we have already established for this manuscript
651 (<https://hdl.handle.net/10217/185610>). This is Lamont contribution number...

652 **References**

- 653 Alvarado, M. J., and 35 others: Nitrogen oxides and PAN in plumes from boreal fires during ARCTAS-B
654 and their impact on ozone: an integrated analysis of aircraft and satellite observations, *Atmos. Chem.*
655 *Phys.*, 10, 9739–9760, doi:10.5194/acp-10-9739-2010, 2010.
- 656 Arnold, S. R., Emmons, L. K., Monks, S. A., Law, K. S., Ridley, D. A., Turquety, S., Tilmes, S., Thomas,
657 J. L., Bouarar, I., Flemming, J., Huijnen, V., Mao, J., Duncan, B. N., Steenrod, S., Yoshida, Y.,
658 Langner, J., and Long, Y.: Biomass burning influence on high-latitude tropospheric ozone and reactive



- 659 nitrogen in summer 2008: a multi-model analysis based on POLMIP simulations, *Atmos. Chem. Phys.*,
660 15, 6047-6068, <https://doi.org/10.5194/acp-15-6047-2015>, 2015.
- 661 Balzani Lööv, J. M., S. Henne, G. Legreid, J. Staehelin, S. Reimann, A. S. H. Prévôt, M. Steinbacher, and
662 M. K. Vollmer: Estimation of background concentrations of trace gases at the Swiss Alpine site
663 Jungfrauoch (3580 m asl), *J. Geophys. Res.*, 113, D22305, doi:[10.1029/2007JD009751](https://doi.org/10.1029/2007JD009751), 2008.
- 664 Bottenheim, J. W., Sirois, A., Brice, K. A., and Gallant, A. J.: Five years of continuous observations of
665 PAN and ozone at a rural location in eastern Canada, *Journal of Geophysical Research: Atmospheres*,
666 99, 5333-5352, [10.1029/93JD02716](https://doi.org/10.1029/93JD02716), 1994.
- 667 Carpenter, L. J., Green, T. J., Mills, G. P., Bauguitte, S., Penkett, S. A., Zanis, P., Schuepbach, E.,
668 Schmidbauer, N., Monks, P. S., Zellweger, C: Oxidized nitrogen and ozone production efficiencies in
669 the springtime free troposphere over the Alps, *J. Geophys. Res.*, 105, D11, 14,547-14,559, 2000.
- 670 Chameides, W. L., Fehsenfeld, F. C., Rodgers, M. O., Cardelino, C., Martinez, J., Parrish, D., Lonnerman,
671 W., Lawson, D. R., Rasmussen, R. A., Zimmerman, P., Greenberg, J., Middleton, P., and Wang, T.:
672 Ozone precursor relationships in the ambient atmosphere, *Journal of Geophysical Research*, 97, 6037-
673 6055, 1992.
- 674 Doherty, R. M., et al.: Impacts of climate change on surface ozone and intercontinental ozone pollution: A
675 multi-model study, *J. Geophys. Res. Atmos.*, 118, doi:[10.1002/jgrd.50266](https://doi.org/10.1002/jgrd.50266), 2013.
- 676 Eckstein, J., Ruhnke, R., Zahn, A., Neumaier, M., Kirner, O., and Braesicke, P.: An assessment of the
677 climatological representativeness of IAGOS-CARIBIC trace gas measurements using EMAC model
678 simulations, *Atmos. Chem. Phys.*, 17, 2775-2794, <https://doi.org/10.5194/acp-17-2775-2017>, 2017.
- 679 Emmerson, K. M., and Evans, M. J.: Comparison of tropospheric gas-phase chemistry schemes for use
680 within global models, *Atmos. Chem. Phys.*, 9, 1831-1845, [10.5194/acp-9-1831-2009](https://doi.org/10.5194/acp-9-1831-2009), 2009.
- 681 Fadnavis, S., Schultz, M. G., Semeniuk, K., Mahajan, A. S., Pozzoli, L., Sonbawne, S., Ghude, S. D.,
682 Kiefer, M., and Eckert, E.: Trends in peroxyacetyl nitrate (PAN) in the upper troposphere and lower
683 stratosphere over southern Asia during the summer monsoon season: regional impacts, *Atmos. Chem.*
684 *Phys.*, 14, 12725-12743, <https://doi.org/10.5194/acp-14-12725-2014>, 2014.
- 685 Fiore, A. M., Dentener, F. J., Wild, O., Cuvelier, C., Schultz, M. G., Hess, P., Textor, C., Schulz, M.,
686 Doherty, R. M., Horowitz, L. W., MacKenzie, I. A., Sanderson, M. G., Shindell, D. T., Stevenson, D.
687 S., Szopa, S., Van Dingenen, R., Zeng, G., Atherton, C., Bergmann, D., Bey, I., Carmichael, G.,
688 Collins, W. J., Duncan, B. N., Faluvegi, G., Folberth, G., Gauss, M., Gong, S., Hauglustaine, D.,
689 Holloway, T., Isaksen, I. S. A., Jacob, D. J., Jonson, J. E., Kaminski, J. W., Keating, T. J., Lupu, A.,
690 Marmer, E., Montanaro, V., Park, R. J., Pitari, G., Pringle, K. J., Pyle, J. A., Schroeder, S., Vivanco,
691 M. G., Wind, P., Wojcik, G., Wu, S., and Zuber, A.: Multimodel estimates of intercontinental source-
692 receptor relationships for ozone pollution, *J. Geophys. Res.*, 114, D04301, [10.1029/2008jd010816](https://doi.org/10.1029/2008jd010816),
693 2009.
- 694 Fiore, A. M., Levy II, H., and Jaffe, D. A.: North American isoprene influence on intercontinental ozone
695 pollution, *Atmos. Chem. Phys.*, 11, 1697-1710, [10.5194/acp-11-1697-2011](https://doi.org/10.5194/acp-11-1697-2011), 2011.



- 696 Fischer, E. V., Jaffe, D. A., Reidmiller, D. R., and Jaegle, L.: Meteorological controls on observed
697 peroxyacetyl nitrate (PAN) at Mount Bachelor during the spring of 2008, *Journal of Geophysical*
698 *Research*, 115 doi: 10.1029/2009JD20012776, 2010.
- 699 Fischer, E. V., Jaffe, D. A., and Weatherhead, E. C.: Free tropospheric peroxyacetyl nitrate (PAN) and
700 ozone at Mount Bachelor: potential causes of variability and timescale for trend detection, *Atmos.*
701 *Chem. Phys.*, 11, 5641-5654, 10.5194/acp-11-5641-2011, 2011.
- 702 Fischer, E. V., Jacob, D. J., Yantosca, R. M., Sulprizio, M. P., Millet, D. B., Mao, J., Paulot, F., Singh, H.
703 B., Roiger, A., Ries, L., Talbot, R. W., Dzepina, K., and Pandey Deolal, S.: Atmospheric peroxyacetyl
704 nitrate (PAN): a global budget and source attribution, *Atmos. Chem. Phys.*, 14, 2679-2698,
705 10.5194/acp-14-2679-2014, 2014.
- 706 Gilge, S., Plass-Dülmer, C., Fricke, W., Kaiser, A., Ries, L., Buchmann, B., and Steinbacher, M.: Ozone,
707 carbon monoxide and nitrogen oxides time series at four alpine GAW mountain stations in central
708 Europe, *Atmos. Chem. Phys.*, 10, 12295-12316, 10.5194/acp-10-12295-2010, 2010.
- 709 Heald, C. L., Jacob, D. J., Fiore, A. M., Emmons, L. K., Gille, J. C., Deeter, M. N., Warner, J., Edwards,
710 D. P., Crawford, J. H., Hamlin, A. J., Sachse, G. W., Browell, E. V., Avery, M. A., Vay, S. A.,
711 Westberg, D. J., Blake, D. R., Singh, H. B., Sandholm, S. T., Talbot, R. W., and Fuelberg, H. E.: Asian
712 outflow and trans-Pacific transport of carbon monoxide and ozone pollution: An integrated satellite,
713 aircraft, and model perspective, *J. Geophys. Res.*, 108, 4804, 10.1029/2003jd003507, 2003.
- 714 Hilboll, A., Richter, A., and Burrows, J.P.: Long-term changes of tropospheric NO₂ over megacities
715 derived from multiple satellite instruments, *Atmos. Chem. Phys.*, 13, 4145-4169, doi:10.5194/acp-13-
716 4145-2013, 2013.
- 717 Honrath, R. E., Owen, R. C., Val Martín, M., Reid, J. S., Lapina, K., Fialho, P., Dziobak, M. P., Kleissl,
718 J., and Westphal, D. L.: Regional and hemispheric impacts of anthropogenic and biomass burning
719 emissions on summertime CO and O₃ in the North Atlantic lower free troposphere, *J. Geophys. Res.*,
720 109, D24310, 10.1029/2004jd005147, 2004.
- 721 HTAP: Task Force on Hemispheric Transport of Air Pollution 2007 Interim Report, United Nations
722 Economic Commission for Europe, New York and Geneva, 2007.
- 723 HTAP: HEMISPHERIC TRANSPORT OF AIR POLLUTION 2010 PART A: OZONE AND
724 PARTICULATE MATTER, Air Pollution Studies No. 17, UNITED NATIONS, New York, 2010.
- 725 Hudman, R. C., Jacob, D. J., Cooper, O. R., Evans, M. J., Heald, C. L., Park, R. J., Fehsenfeld, F., Flocke,
726 F., Holloway, J., Hübler, G., Kita, K., Koike, M., Kondo, Y., Neuman, A., Nowak, J., Oltmans, S.,
727 Parrish, D., Roberts, J. M., and Ryerson, T.: Ozone production in transpacific Asian pollution plumes
728 and implications for ozone air quality in California, *J. Geophys. Res.*, 109, D23S10,
729 10.1029/2004jd004974, 2004.
- 730 Jaeglé, L., Jaffe, D. A., Price, H. U., Weiss-Penzias, P., Palmer, P. I., Evans, M. J., Jacob, D. J., and Bey,
731 I.: Sources and budgets for CO and O₃ in the northeastern Pacific during the spring of 2001: Results



- 732 from the PHOBEA-II Experiment, *Journal of Geophysical Research*, 108, doi:10.1029/2002JD003121,
733 2003.
- 734 Jaffe, D., Thornton, J., Wolfe, G., Reidmiller, D., Fischer, E. V., Jacob, D. J., Cohen, R., Singh, H.,
735 Weinheimer, A., and Flocke, F.: Can we Detect an Influence over North America From Increasing
736 Asian NO_x Emissions?, *EOS Trans. AGU*, 88(52), Fall Meet. Suppl., Abstract A51E-04, 2007.
- 737 Jiang, Z., Worden, J. R., Payne, V. H., Zhu, L., Fischer, E., Walker, T., and Jones, D. B. A.: Ozone export
738 from East Asia: The role of PAN, *Journal of Geophysical Research: Atmospheres*, 121, 6555-6563,
739 10.1002/2016JD024952, 2016.
- 740 Jonson, J. E., Stohl, A., Fiore, A. M., Hess, P., Szopa, S., Wild, O., Zeng, G., Dentener, F. J., Lupu, A.,
741 Schultz, M. G., Duncan, B. N., Sudo, K., Wind, P., Schulz, M., Marmer, E., Cuvelier, C., Keating, T.,
742 Zuber, A., Valdebenito, A., Dorokhov, V., De Backer, H., Davies, J., Chen, G. H., Johnson, B.,
743 Tarasick, D. W., Stübi, R., Newchurch, M. J., von der Gathen, P., Steinbrecht, W., and Claude, H.: A
744 multi-model analysis of vertical ozone profiles, *Atmos. Chem. Phys.*, 10, 5759-5783, 10.5194/acp-10-
745 5759-2010, 2010.
- 746 Kaiser, A., Scheifinger, H., Spangl, W., Weiss, A., Gilge, S., Fricke, W., Ries, L., Cemas, D., and
747 Jesenovec, B.: Transport of nitrogen oxides, carbon monoxide and ozone to the Alpine Global
748 Atmosphere Watch stations Jungfraujoch (Switzerland), Zugspitze and Hohenpeissenberg (Germany),
749 Sonnblick (Austria) and Mt. Kravec (Slovenia), *Atmospheric Environment*, 41, 9273-9287,
750 <https://doi.org/10.1016/j.atmosenv.2007.09.027>, 2007.
- 751 Kirchner, F., Mayer-Figge, A., Zabel, F., and Becker, K. H.: Thermal stability of peroxy nitrates,
752 *International Journal of Chemical Kinetics*, 31, 127-144, 1999.
- 753 Kotchenruther, R. A., Jaffe, D. A., and Jaeglé, L.: Ozone photochemistry and the role of PAN in the
754 springtime northeastern Pacific Troposphere: Results from the PHOBEA Campaign. *J. Geophys. Res.*,
755 106, 28731-28741, 2001a.
- 756 Kotchenruther, R. A., Jaffe, D. A., Beine, H. J., Anderson, T., Bottenheim, J. W., Harris, J. M., Blake, D.,
757 and Schmitt, R.: Observations of ozone and related species in the Northeast Pacific during the
758 PHOBEA Campaigns: 2. Airborne observations. *J. Geophys. Res.*, 106, 7463-7483, 2001b (corrected
759 Table 1 published in Vol. 106 (D17), p.20507).
- 760 Koumoutsaris, S., Bey, I., Generoso, S., and Thouret, V.: Influence of El Niño-Southern Oscillation on the
761 interannual variability of tropospheric ozone in the northern midlatitudes, *J. Geophys. Res.*, 113,
762 D19301, 10.1029/2007jd009753, 2008.
- 763 Kuhn, M., Builtjes, P. J. H., Poppe, D., Simpson, D., Stockwell, W. R., Andersson-Sköld, Y., Baart, A.,
764 Das, M., Fiedler, F., Hov, Ø., Kirchner, F., Makar, P. A., Milford, J. B., Roemer, M. G. M., Ruhnke,
765 R., Strand, A., Vogel, B., and Vogel, H.: Intercomparison of the gas-phase chemistry in several
766 chemistry and transport models, *Atmospheric Environment*, 32, 693-709, 1998.



- 767 Liang, J., Horowitz, L. W., Jacob, D. J., Wang, Y., Fiore, A. M., Logan, J. A., Gardner, G. M., and
768 Munger, J. W.: Seasonal variations of reactive nitrogen species and ozone over the United States and
769 export fluxes to the global atmosphere, *Journal of Geophysical Research*, 103, 13,435-413,450, 1998.
- 770 Lin, M., Holloway, T., Carmichael, G. R., and Fiore, A. M.: Quantifying pollution inflow and outflow
771 over East Asia in spring with regional and global models, *Atmos. Chem. Phys.*, 10, 4221-4239,
772 10.5194/acp-10-4221-2010, 2010.
- 773 Liu, S. C., Trainer, M., Fehsenfeld, F. C., Parrish, D. D., Williams, E. J., Fahey, D. W., Hubler, G., and
774 Murphy, P. C.: Ozone production in the Rural Troposphere and the Implications for Regional and
775 Global Ozone Distributions, *Journal of Geophysical Research*, 92, 4191-4207, 1987.
- 776 Moxim, W. J., Levy, H., II, and Kasibhatla, P. S.: Simulated global tropospheric PAN: Its transport and
777 impact on NO_x, *J. Geophys. Res.*, 101, 12621-12638, 10.1029/96jd00338, 1996.
- 778 Naja, M., H. Akimoto, and J. Staehelin: Ozone in background and photochemically aged air over central
779 Europe: Analysis of long-term ozonesonde data from Hohenpeissenberg and Payerne, *J. Geophys.
780 Res.*, 108, 4063, doi:[10.1029/2002JD002477](https://doi.org/10.1029/2002JD002477), D2, 2003.
- 781 Orbe, C., D. W. Waugh, H. Yang, J.-F. Lamarque, S. Tilmes, and D. E. Kinnison (2017), Tropospheric
782 transport differences between models using the same large-scale meteorological fields, *Geophys. Res.
783 Lett.*, 44, 1068–1078, doi:10.1002/2016GL071339.
- 784 Pandey Deolal, S., Henne, S., Ries, L., Gilge, S., Weers, U., Steinbacher, M., Staehelin, J., and Peter, T.:
785 Analysis of elevated springtime levels of Peroxyacetyl nitrate (PAN) at the high Alpine research sites
786 Jungfraujoch and Zugspitze, *Atmos. Chem. Phys.*, 14, 12553-12571, 10.5194/acp-14-12553-2014,
787 2014.
- 788 Pandey Deolal, S., Staehelin, J., Brunner, D., Cui, J., Steinbacher, M., Zellweger, C., Henne, S., and
789 Vollmer, M. K.: Transport of PAN and NO_y from different source regions to the Swiss high alpine site
790 Jungfraujoch, *Atmospheric Environment*, 64, 103-115,
791 <https://doi.org/10.1016/j.atmosenv.2012.08.021>, 2013.
- 792 Pätz, H.-W., Corsmeier, U., Glaser, K., Vogt, U., Kalthoff, N., Klemp, D., Kolahgar, B., Lerner, A.,
793 Neininger, B., Schmitz, T., Schultz, M. G., Slemr, J., and Volz-Thomas, A.: Measurements of trace
794 gases and photolysis frequencies during SLOPE96 and a coarse estimate of the local OH concentration
795 from HNO₃ formation, *Journal of Geophysical Research: Atmospheres*, 105, 1563-1583,
796 10.1029/1999JD900918, 2000.
- 797 Payne, V. H., Alvarado, M. J., Cady-Pereira, K. E., Worden, J. R., Kulawik, S. S., and Fischer, E. V.:
798 Satellite observations of peroxyacetyl nitrate from the Aura Tropospheric Emission Spectrometer,
799 *Atmos. Meas. Tech.*, 7, 3737-3749, 10.5194/amt-7-3737-2014, 2014.
- 800 Payne, V. H., Fischer, E. V., Worden, J. R., Jiang, Z., Zhu, L., Kurosu, T. P., and Kulawik, S. S.: Spatial
801 variability in tropospheric peroxyacetyl nitrate in the tropics from infrared satellite observations in
802 2005 and 2006, *Atmos. Chem. Phys.*, 17, 6341-6351, 10.5194/acp-17-6341-2017, 2017.



- 803 Penkett, S. A., and Brice, K. A.: The spring maximum in photo-oxidants in the Northern Hemisphere
804 troposphere, *Nature*, 319, 655-657, 1986.
- 805 Petzold A., V. Thouret, C. Gerbig, A. Zahn, C.A.M. Brenninkmeijer, M. Gallagher, M. Hermann, M.
806 Pontaud, H. Ziereis, D. Boulanger, J. Marshall, P. Nédélec, H.G.J. Smit, U. Frieß, J.-M. Flaud, A.
807 Wahner, J.-P. Cammas, A. Volz-Thomas, and IAGOS Team: Global-Scale Atmosphere Monitoring by
808 In-Service Aircraft - Current Achievements and Future Prospects of the European Research
809 Infrastructure IAGOS, *Tellus-B*, 67, 28452, doi:10.3402/tellusb.v67.28452, 2015.
- 810 Real, E., Orlandi, E., Law, K. S., Fierli, F., Josset, D., Cairo, F., Schlager, H., Borrmann, S., Kunkel, D.,
811 Volk, C. M., McQuaid, J. B., Stewart, D. J., Lee, J., Lewis, A. C., Hopkins, J. R., Ravegnani, F.,
812 Ulanovski, A., and Lioussé, C.: Cross-hemispheric transport of central African biomass burning
813 pollutants: implications for downwind ozone production, *Atmos. Chem. Phys.*, 10, 3027-3046,
814 <https://doi.org/10.5194/acp-10-3027-2010>, 2010.
- 815 Roberts, J. M.: PAN and Related Compounds, in: *Volatile Organic Compounds in the Atmosphere*, edited
816 by: Koppmann, R., Blackwell Publishing, 500, 2007.
- 817 Roberts, J. M., Marchewka, M., Bertman, S. B., Goldan, P., Kuster, W., de Gouw, J., Warneke, C.,
818 Williams, E., Lerner, B., Murphy, P., Apel, E., and Fehsenfeld, F. C.: Analysis of the isoprene
819 chemistry observed during the New England Air Quality Study (NEAQS) 2002 intensive experiment,
820 *Journal of Geophysical Research: Atmospheres*, 111, D23S12, 10.1029/2006JD007570, 2006.
- 821 Schmitt, R., and Volz-Thomas, A.: Climatology of Ozone, PAN, CO, and NMHC in the Free Troposphere
822 Over the Southern North Atlantic, *Journal of Atmospheric Chemistry*, 28, 245-262,
823 10.1023/A:1005801515531, 1997.
- 824 Schultz, M., Rast, S., van het Bolscher, M., Pulles, T., Brand, R., Pereira, J., Mota, B., Spessa, A.,
825 Dalsoren, S., van Noije, T., and Szopa, S.: Emission data sets and methodologies for estimating
826 emissions, Hamburg, 2007.
- 827 Schultz, M. G., Heil, A., Hoelzemann, J. J., Spessa, A., Thonicke, K., Goldammer, J. G., Held, A. C.,
828 Pereira, J. M. C., and van het Bolscher, M.: Global wildland fire emissions from 1960 to 2000, *Global*
829 *Biogeochemical Cycles*, 22, GB2002, 10.1029/2007GB003031, 2008.
- 830 Schultz MG, Schröder S, Lyapina O, Cooper O, Galbally I, Petropavlovskikh I, et al.: Tropospheric Ozone
831 Assessment Report: Database and Metrics Data of Global Surface Ozone Observations, *Elem Sci*
832 *Anth.*, 5, 58, DOI: <http://doi.org/10.1525/elementa.244>, 2017.
- 833 Shindell, D. T., Chin, M., Dentener, F., Doherty, R. M., Faluvegi, G., Fiore, A. M., Hess, P., Koch, D. M.,
834 MacKenzie, I. A., Sanderson, M. G., Schultz, M. G., Schulz, M., Stevenson, D. S., Teich, H., Textor,
835 C., Wild, O., Bergmann, D. J., Bey, I., Bian, H., Cuvelier, C., Duncan, B. N., Folberth, G., Horowitz,
836 L. W., Jonson, J., Kaminski, J. W., Marmer, E., Park, R., Pringle, K. J., Schroeder, S., Szopa, S.,
837 Takemura, T., Zeng, G., Keating, T. J., and Zuber, A.: A multi-model assessment of pollution transport
838 to the Arctic, *Atmos. Chem. Phys.*, 8, 5353-5372, 10.5194/acp-8-5353-2008, 2008.



- 839 Singh, H. B.: Reactive nitrogen in the troposphere, *Environmental Science and Technology*, 21, 320-327,
840 1987.
- 841 Singh, H. B., and Hanst, P. L.: Peroxyacetyl nitrate (PAN) in the unpolluted atmosphere: An important
842 reservoir for nitrogen oxides, *Geophysical Research Letters*, 8, 941-944, 1981.
- 843 Singh, H. B., and Salas, L. J.: Measurements of peroxyacetyl nitrate (pan) and peroxypropionyl nitrate
844 (ppn) at selected urban, rural and remote sites, *Atmospheric Environment* (1967), 23, 231-238,
845 [https://doi.org/10.1016/0004-6981\(89\)90115-7](https://doi.org/10.1016/0004-6981(89)90115-7), 1989.
- 846 Stohl, A.: Computation, accuracy and applications of trajectories—A review and bibliography,
847 *Atmospheric Environment*, 32, 947-966, [https://doi.org/10.1016/S1352-2310\(97\)00457-3](https://doi.org/10.1016/S1352-2310(97)00457-3), 1998.
- 848 Turnipseed, A. A., Huey, L. G., Nemitz, E., Stickel, R., Higgs, J., Tanner, D. J., Slusher, D. L., Sparks, J.
849 P., Flocke, F., and Guenther, A.: Eddy covariance fluxes of peroxyacetyl nitrates (PANs) and NO_y to a
850 coniferous forest, *Journal of Geophysical Research: Atmospheres*, 111, D09304,
851 [10.1029/2005jd006631](https://doi.org/10.1029/2005jd006631), 2006.
- 852 Val Martin, M., Honrath, R. E., Owen, R. C., and Lapina, K.: Large-scale impacts of anthropogenic
853 pollution and boreal wildfires on the nitrogen oxide levels over the central North Atlantic region,
854 *Journal of Geophysical Research*, 113, doi:10.1029/2007JD009689, 2008a.
- 855 Val Martin, M., Honrath, R. E., Owen, R. C., and Li, Q. B.: Seasonal variation of nitrogen oxides in the
856 central North Atlantic lower free troposphere, *J. Geophys. Res.*, 113, D17307, [10.1029/2007jd009688](https://doi.org/10.1029/2007jd009688),
857 2008b.
- 858 van der Werf, G. R., Randerson, J. T., Giglio, L., Collatz, G. J., Kasibhatla, P. S., and Arellano Jr, A. F.:
859 Interannual variability in global biomass burning emissions from 1997 to 2004, *Atmos. Chem. Phys.*,
860 6, 3423-3441, [10.5194/acp-6-3423-2006](https://doi.org/10.5194/acp-6-3423-2006), 2006.
- 861 van der Werf, G. R., Randerson, J. T., Giglio, L., Collatz, G. J., Mu, M., Kasibhatla, P. S., Morton, D. C.,
862 DeFries, R. S., Jin, Y., and van Leeuwen, T. T.: Global fire emissions and the contribution of
863 deforestation, savanna, forest, agricultural, and peat fires (1997–2009), *Atmos. Chem. Phys.*, 10,
864 11707-11735, [10.5194/acp-10-11707-2010](https://doi.org/10.5194/acp-10-11707-2010), 2010.
- 865 Volz-Thomas, A., Xueref, I., and Schmitt, R.: An automatic gas chromatograph and calibration system for
866 ambient measurements of PAN and PPN, *Environmental Science and Pollution Resources*, Special
867 Issue 4, 72-76, 2002.
- 868 Wang, Y., and Jacob, D. J.: Anthropogenic forcing on tropospheric ozone and OH since preindustrial
869 times, *Journal of Geophysical Research*, 103, 31,123-131,135, 1998.
- 870 Warneck, P., and Zerbach, T.: Synthesis of peroxyacetyl nitrate by acetone photolysis, *Environmental*
871 *Science and Technology*, 26, 74-79, 1992.
- 872 Weiss-Penzias, P., Jaffe, D. A., Jaeglé, L., and Liang, Q.: Influence of long-range-transported pollution on
873 the annual and diurnal cycles of carbon monoxide and ozone at Cheeka Peak Observatory, *Journal of*
874 *Geophysical Research: Atmospheres*, 109, n/a-n/a, [10.1029/2004JD004505](https://doi.org/10.1029/2004JD004505), 2004.



- 875 Wild, O., Fiore, A. M., Shindell, D. T., Doherty, R. M., Collins, W. J., Dentener, F. J., Schultz, M. G.,
876 Gong, S., MacKenzie, I. A., Zeng, G., Hess, P., Duncan, B. N., Bergmann, D. J., Szopa, S., Jonson, J.
877 E., Keating, T. J., and Zuber, A.: Modelling future changes in surface ozone: a parameterized
878 approach, *Atmos. Chem. Phys.*, 12, 2037-2054, [10.5194/acp-12-2037-2012](https://doi.org/10.5194/acp-12-2037-2012), 2012.
- 879 Wolfe, G. M., Thornton, J. A., Yatavelli, R. L. N., McKay, M., Goldstein, A. H., LaFranchi, B., Min, K.
880 E., and Cohen, R. C.: Eddy covariance fluxes of acyl peroxy nitrates (PAN, PPN and MPAN) above a
881 Ponderosa pine forest, *Atmospheric Chemistry and Physics*, 9, 615-634, 2009.
- 882 Wu, S., Duncan, B. N., Jacob, D. J., Fiore, A. M., and Wild, O.: Chemical nonlinearities in relating
883 intercontinental ozone pollution to anthropogenic emissions, *Geophys. Res. Lett.*, 36, L05806,
884 [10.1029/2008gl036607](https://doi.org/10.1029/2008gl036607), 2009.
- 885 Zellweger, C., Ammann, M., Buchmann, B., Hofer, P., Lugauer, M., Rüttimann, R., Streit, N.,
886 Weingartner, E., and Baltensperger, U.: Summertime NO_y speciation at the Jungfrauoch, 3580 m asl,
887 Switzerland, *Journal of Geophysical Research*, 105, 2000.
- 888 Zellweger, C., Forrer, J., Hofer, P., Nyeki, S., Schwarzenbach, B., Weingartner, E., Ammann, M., and
889 Baltensperger, U.: Partitioning of reactive nitrogen (NO_y) and dependence on meteorological
890 conditions in the lower free troposphere, *Atmospheric Chemistry and Physics*, 3, 779-796, 2003.
- 891 Zhang, L., Jacob, D. J., Boersma, K. F., Jaffe, D. A., Olson, J. R., Bowman, K. W., Worden, J. R.,
892 Thompson, A. M., Avery, M. A., Cohen, R. C., Dibb, J. E., Flocke, F. M., Fuelberg, H. E., Huey, L.
893 G., McMillian, W. W., Singh, H. B., and Weinheimer, A. J.: Transpacific transport of ozone pollution
894 and the effect of recent Asian emission increases on air quality in North America: an integrated
895 analysis using satellite, aircraft, ozonesonde, and surface observations, *Atmospheric Chemistry and*
896 *Physics*, 8, 6117-6136, 2008.
- 897 Zhu, L., Fischer, E. V., Payne, V. H., Worden, J. R., and Jiang, Z.: TES observations of the interannual
898 variability of PAN over Northern Eurasia and the relationship to springtime fires, *Geophysical*
899 *Research Letters*, 42, 7230-7237, [10.1002/2015GL065328](https://doi.org/10.1002/2015GL065328), 2015.
- 900
- 901


 902 **Table 1: Specifications of individual models contributing to the HTAP1 simulations (SR1, SR6xx, and**
 903 **COfromXX) used in this study.**

Model	Resolution (lat-lon- layers)	Institute	Model contact	SR1	SR6xx	COfromXX
CAMCHEM-3311m13	2.5°x2°x30	NCAR, USA	Peter Hess	X	X	X
FRSGUCI-v01	2.81°x2.81° x37	Lancaster University, UK	Oliver Wild	X	X	X
GEMAQ-v1p0	2°x2°x28	York University, Canada	Alex Lupu	X	X	X
GEOSChem-v07	2.5°x2°x30	Harvard University, USA	Rokjin Park	X	X	X
GISS-PUCCINI- modelE	5°x4°x23	NASA GISS, USA	Drew Shindell	X	X	X
GMI-v02f	2.5°x2°x42	NASA GSFC, USA	Bryan Duncan	X	X	X
LMDZ3-INCA1	3.75° x 2° x 19	CEA, France	Sophie Szopa	X	X	
LLNL-IMPACT- T5a	2.5° x 2° x 48	LLNL, USA	Dan Bergmann	X		
MOZARTGFDL- v2	1.88° x 1.88° x 28	NOAA GFDL, USA	Arlene Fiore	X	X	X
MOZECH-v16	1.88° x 1.88° x 28	FZ Julich, Germany	Martin Schultz	X	X	X
STOC-HadAM3- v01	5° x 5° x 19	University of Edinburg, UK	Ruth Doherty, David Stevenson	X	X	X
STOCHEM-v02	3.75 x 2.5° x 20	Met Office, Hadley Center, UK	Bill Collins, Michael Sanderson	X		
TM5-JRC-cy2- ipcc-v1	1° x 1° x 25	JRC, Italy	Frank Dentener	X	X	X



UM-CAM-v01	3.75° x 2.5° x 19	University of Cambridge, UK	Guang Zeng	X	X	X
------------	----------------------	--------------------------------	------------	---	---	---

904

905

906

907

908

909

910

911

912

913

914

915

916



917 **Table 2: Simulations from the HTAP1 multi-model intercomparison used in this study.**

Simulation	Description
SR1	Base case (see Section 2.1 for details)
SR6EA	SR1 but with anthropogenic emissions of all O ₃ precursors (NO _x +CO+NMVOC) and aerosols within EA decreased by 20%
SR6EU	SR1 but with 20% emissions reductions within the EU region
SR6NA	SR1 but with 20% emissions reductions within the NA region.
ISOPNA	SR1 but with a 20% increase in NA isoprene emissions (MOZARTGFDL-v2 model only)
COfromEA	Idealized tracer simulation in which all models use identical CO emissions, emitted within the EA region, with a 50-day e-folding lifetime.
COfromEU	Same as COfromEA but for the EU region.
COfromNA	Same as COfromEA but for the NA region.

918

919

920

921

922



923 **Table 3: PAN observations at mountain sites in the northern hemisphere mid-latitudes used in this study.**

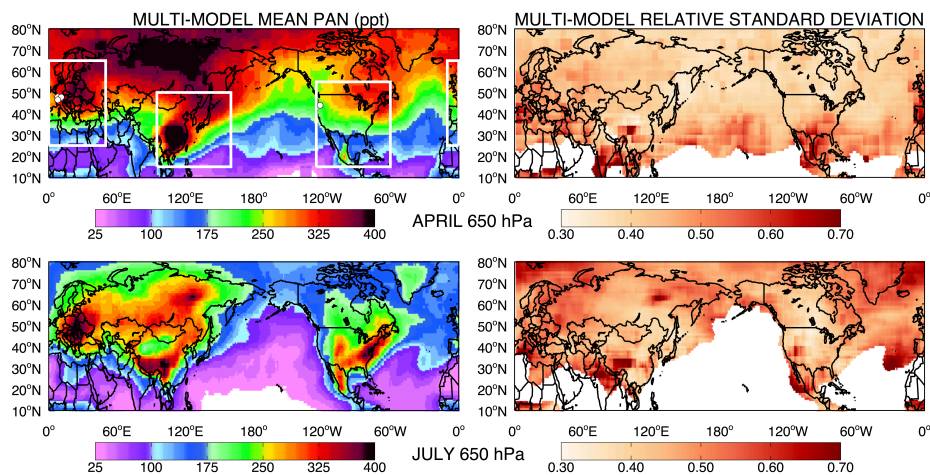
Site	Location	Elevation	Measurement Period (s)	Reference (s)
Mount Bachelor	43.979° N, 121.687° W	2763m	3 April – 18 June 2008, 30 August – 7 October 2008, 26 March – 20 May 2009, 23 March – 25 May 2010	(Fischer et al., 2010; Fischer et al., 2011)
Hohenpeissenberg	47.80° N, 11.02° E	985 m	January 2003 – December 2008	http://www.dwd.de/de/GAW (Gilge et al., 2010)
Jungfrauoch	46.55°N, 7.98°E	3580 m	April 1997 – May 1998, Aug 30 2005 – Sept 16 2005, Throughout 2005, but not continuous	(Balzani Lööv et al., 2008; Carpenter et al., 2000; Zellweger et al., 2000; Zellweger et al., 2003)
Zugspitze	47.42° N, 10.98° E	2960 m	May 2004 – December 2008	http://gaw.kishou.go.jp
Schauinsland	47.92° N, 7.92° E	1205m	January 1995 – December 2010	www.umweltbundesamt.de

924

925



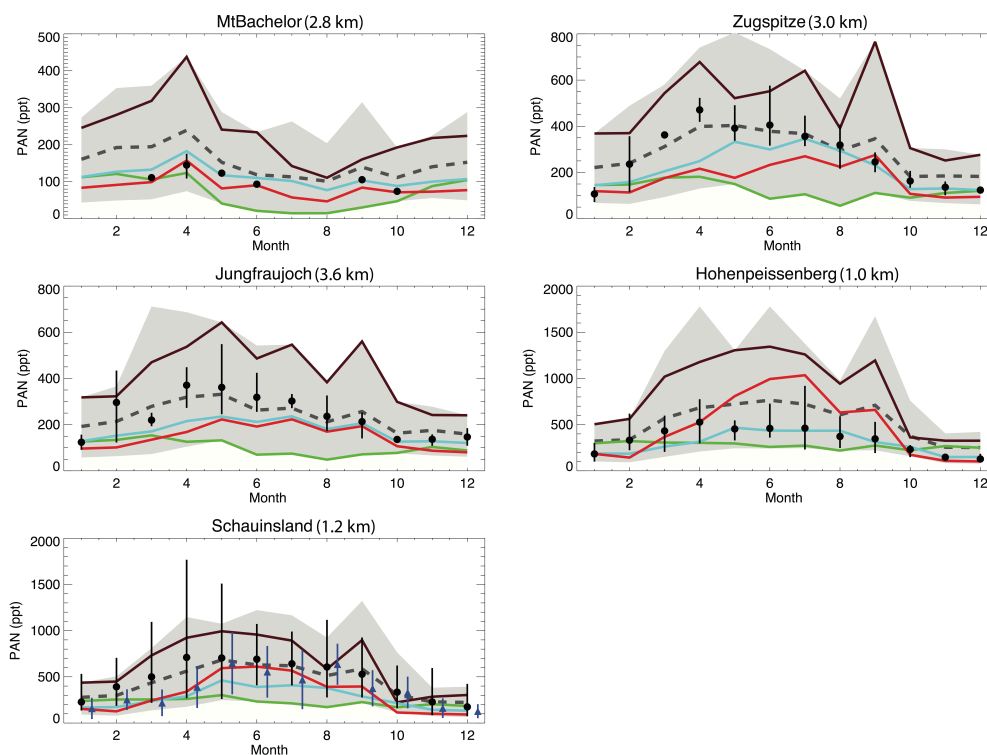
926
927
928



929

930 **Figure 1:** Multi-model ensemble (n=14; Table 1) average PAN mixing ratios (ppt; left panels) and relative
931 standard deviation (the absolute standard deviation across the models divided by the ensemble mean; right
932 panels) at 650 hPa in April and July; relative standard deviations are masked out (white) for regions where
933 multi-model mean PAN falls below 100 ppt. The models were sampled at 650 hPa by vertically interpolating
934 between the bounding grid cells and then re-gridded horizontally to a common 1°x1° grid. White lines denote
935 the HTAP1 source regions: Europe and North Africa (EU), East Asia (EA) and North America (NA) from left to
936 right, and white circles indicate the five mountain sites used in our analysis (Zugspitze and Hohenpeissenberg
937 are too close to differentiate on the map; see Table 3).

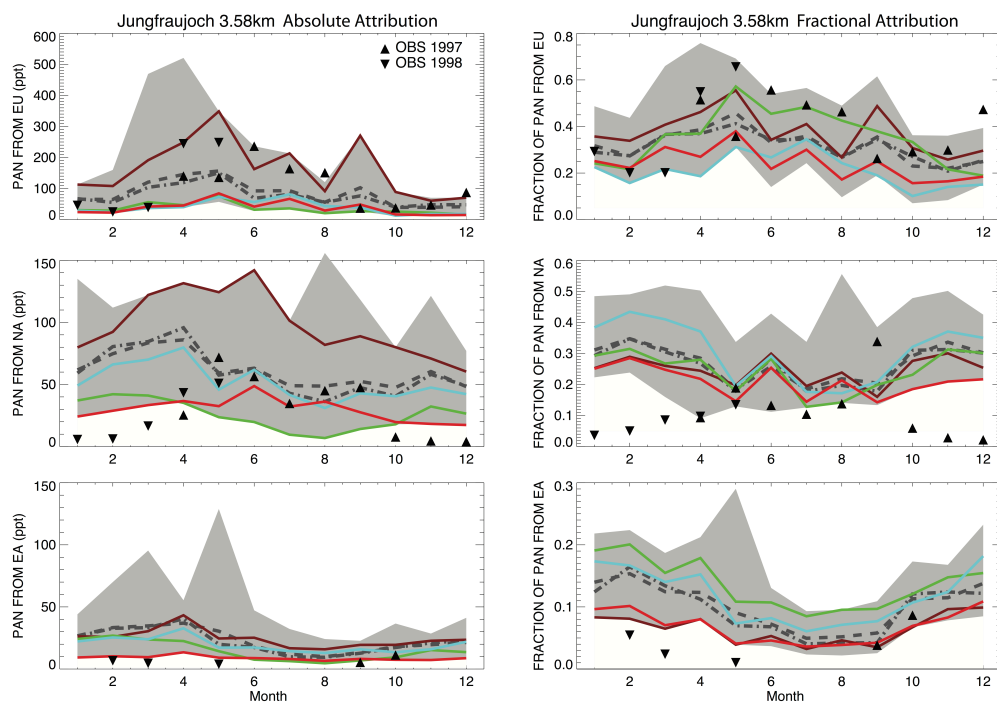
938
939
940
941



942

943 **Figure 2: Monthly mean observed (black symbols for the multiyear mean, with minimum and maximum across**
944 **the available years shown as black vertical lines; see Table 3) and simulated (the 14-model mean is shown as the**
945 **grey dashed line; grey shading encompasses maximum and minimum values from any model in each month)**
946 **PAN at northern mid-latitude mountain sites with multiple years of PAN measurements. For illustrative**
947 **purposes, we show a “high” model (CAM-Chem, brown), a “low” model (GISS-ModelE, green), and two models**
948 **that vary from site to site in their comparison to the other models (MOZARTGFDL, red and GMI, cyan). Also**
949 **shown are year 2001 monthly mean values available at the Schauinsland site (blue triangles offset by a few days**
950 **for clarity) and the standard deviation of measurements within each month (blue vertical lines).**

951



952

953

954 **Figure 3: Absolute (left) and fractional (right) mixing ratios of PAN at Jungfraujoch attributed to EU (top), NA**
955 **(middle) and EA (bottom) precursor emissions by the HTAP1 models ((SR1-SR6XX)*5 for comparison with**
956 **trajectory-based estimates; see Table 1). Shown are the 12-model mean (dashed), median (dot-dashed) and**
957 **range (gray shading). Selected individual models are colored as in Figure 2. Also shown are the trajectory-**
958 **based attributions (solid triangles; Section 2.3). See Section 4 for details.**

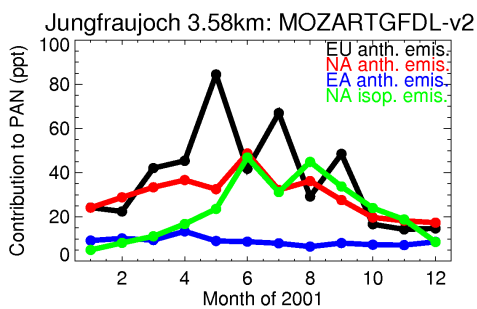
959

960

961



962



963

964 **Figure 4: Contribution to PAN mixing ratios at Jungfraujoch from EU (black), NA (red) and EA (blue)**
965 **anthropogenic precursor emissions and from NA isoprene emissions (green) in the MOZARTGFDL model. We**
966 **take the difference between the base simulation and one in which emissions are decreased by 20% for the**
967 **anthropogenic cases but increased by 20% for isoprene, and then multiply each difference by 5 to estimate a**
968 **100% contribution.**

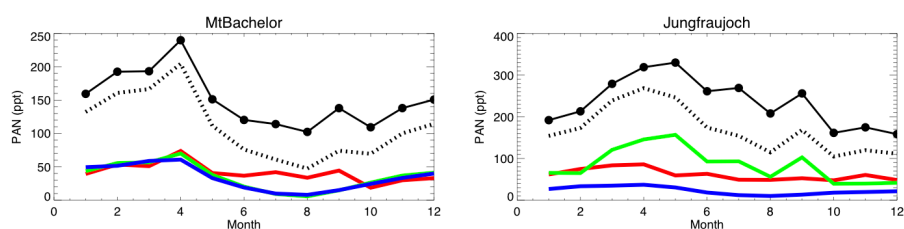
969

970

971



972



973

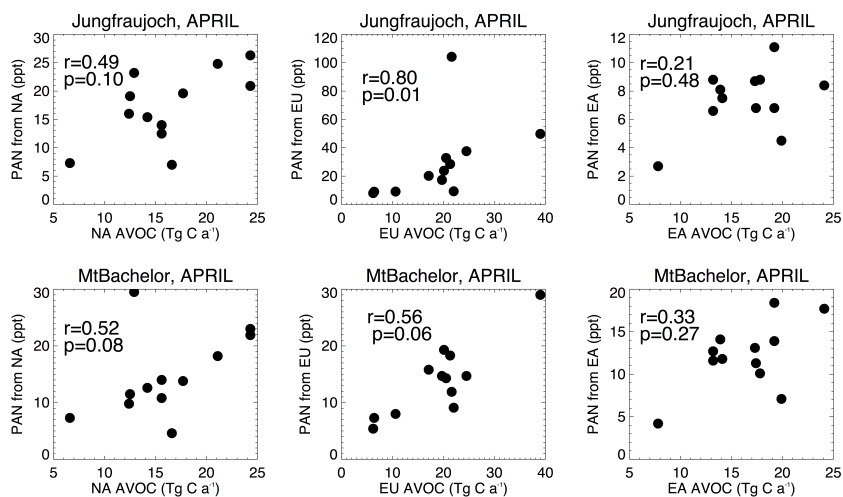
974 **Figure 5: Multi-model monthly mean PAN mixing ratios (black circles) at Mt. Bachelor (left) and Jungfraujoch**
975 **(right). We take the difference between the base simulation and one in which emissions are decreased by 20%**
976 **and then multiply the difference by 5 to estimate a 100% contribution associated with anthropogenic precursor**
977 **emissions from Europe (green), North America (red), East Asia (blue); the sum of the anthropogenic**
978 **contribution from these three regions is also shown (dashed black) for comparison with total simulated PAN**
979 **(solid black).**

980

981



982



983

984 **Figure 6: Source-receptor relationships for PAN (ppt) at Jungfraujoch (top) and Mt. Bachelor (bottom) in each**
985 **HTAP1 model (diagnosed as the difference between the SR1 and SR6xx simulations in Table 1) versus the**
986 **annual emission of anthropogenic VOC (AVOC; Tg C a⁻¹) within the NA (left), EU (middle) and EA (right)**
987 **source regions. The Spearman rank correlation coefficient (more robust to outliers than the traditional Pearson**
988 **coefficient) and associated p-value are shown in each panel.**
989

990

991

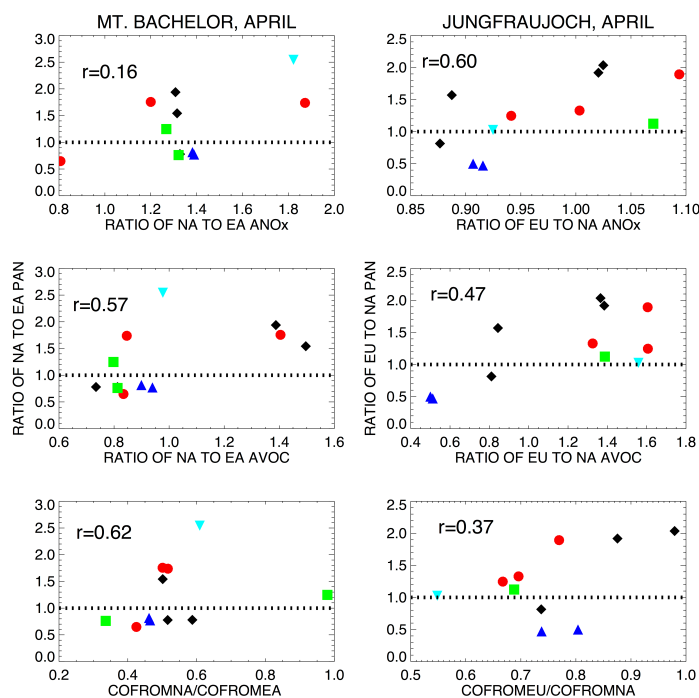
992

993

994

995

996



997

998

999

1000

1001

1002

1003

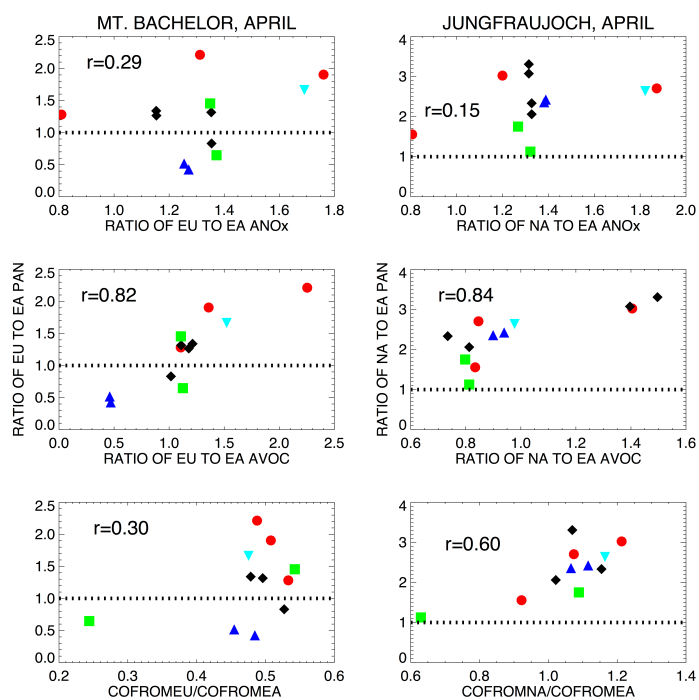
1004

1005

1006

1007

Figure 7: The ratio in April of simulated source-receptor relationships for PAN sampled at Mt. Bachelor (left) or Jungfraujoch (right) produced from emissions within the continental region where the site is located versus an intercontinental region, plotted as a function of the regional-to-intercontinental ratio of anthropogenic NO_x emissions (ANO_x ; top row), of anthropogenic volatile organic compound emissions (AVOC; middle row), or of idealized tracers of model transport (COfromXX where XX = region of origin). Each point corresponds to an individual model and is color-coded by the meteorological fields used in the simulation: blue triangles for GEOS winds; red circles for NCEP; black diamonds for ECMWF; cyan upside-down triangles for CMC; green squares for general circulation models forced by observed sea surface temperatures and sea ice. At Jungfraujoch, one model with a ratio of 8.3 for EU to NA PAN is excluded. The Spearman rank correlation coefficient is shown in each panel.



1008

1009

Figure 8: As in Figure 7, but for ratios between two intercontinental source regions.

1010

1011

1012

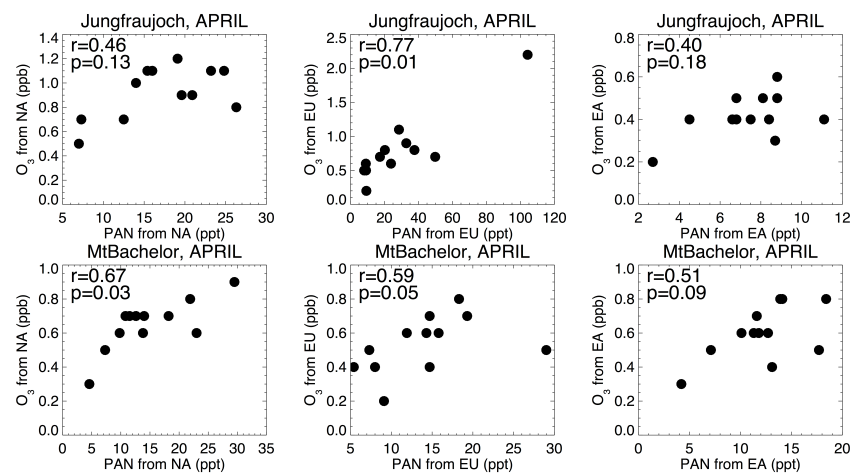
1013

1014

1015

1016

1017



1018

1019

1020 **Figure 9: Source-receptor pairs for O₃ versus PAN at Jungfraujoch (top) and Mt. Bachelor (bottom), obtained**
1021 **from the difference between the SR6XX and SR1 simulations available from 12 models (Table 1), where XX**
1022 **denotes the NA (left), EU (middle) or EA (right) source region. Each model thus contributes one point in each**
1023 **panel. Also shown are the Spearman (rank) correlation coefficient and p-values.**

1024